ISSN 1391-0256

Journal of the Sri Lanka Association for the Advancement of Science

Volume 8 Issue 1, 2026

JSLAAS

Founded in 1944 and incorporated by the Act of Parliament No 11 of 1966

Journal of the Sri Lanka Association for the Advancement of Science is a biannual publication. Selected research work from annual research sessions (based on scientific merit) as well as other research articles are invited to submit research manuscripts as per the guidelines provided by SLAAS. SLAAS members may also separately submit their papers for publication. The Journal can be accessed on-line to view and download the full text of the articles published respective to the volumes free of charge

Submission Manuscript

Only online submission, Web: https://journal.slaas.lk,e-ISSN: 2682-6992

Exchanges: Please address all requests to the Secretary, *Sri Lanka Association for the Advancement of Science, "Vidya Mandiraya" 120/10, Wijerama Mawatha Colombo 07, Sri Lanka*

Table of Contents

Analysis of fat content and fatty acid profile of selected bakery products available in Jaffna district, Sri Lanka

S. Thivya, M. R. Premdharshan and S. Sivakanthan*

Department of Agricultural Chemistry, Faculty of Agriculture, University of Jaffna, Ariviyal Nagar, Kilinochchi, Sri Lanka.

ABSTRACT

High consumption of trans fatty acids and saturated fatty acids is detrimental to human health. Bakery products are among the main sources of these two types of fatty acids in the diets of many people worldwide. The objective of this study was to determine the total fat content and fatty acid profiles of selected bakery products available in Jaffna markets, with a main emphasis on saturated and trans fatty acid contents. Samples such as bread (n=17), bun (n=17), cake (n=16), pastry (n=12), doughnut (n=4), and bakery fats (n=5) were analyzed. The highest fat content was observed in pastries (21.63%-39.83%) and doughnuts (31.66%-37.17%), whereas the lowest fat content was observed in breads (1.00%-3.43%). All bakery products consisted of a considerable amount of elaidic acid. Highest total saturated fatty acid content was detected in pastries (17.25 g/100 g), whereas the lowest was observed in breads (1.36 g/100 g). Highest total trans fatty acid content was detected in pastries (2.47 g/100 g), followed by doughnuts (1.54 g/100 g), cakes (1.03 g/100 g), buns (0.28 g/100 g) and breads (0.08 g/100 g). Significant variations in the fatty acid composition were observed within and between types of products. Therefore, regulations should be imposed to reduce the content of saturated and trans fatty acids in bakery products in Sri Lanka.

Keywords: bread; doughnut; saturated fatty acids; total fat; trans fatty acids

----
* ssubajiny@univ.jfn.ac.lk

INTRODUCTION

Non-communicable diseases (NCDs) continue to pose a formidable global health burden, responsible for nearly three-quarters (74%) of all deaths and an alarming 86% of premature mortality worldwide in 2023 (Varghese et al., 2025). Cardiovascular diseases represent the principal contributor to the global burden of NCDs, responsible for nearly 20.5 million deaths annually (Cesare et al., 2023). In Sri Lanka, ischemic heart disease accounted for 8,550 hospital-reported deaths in 2022 and 8,518 deaths in 2023 per 100,000 population (Ministry of Health Sri Lanka, 2024). One of the major modifiable behavioral risk factors for cardiovascular diseases and other NCDs is the increased consumption of unhealthy diets (WHO, 2025). Therefore, healthy food choices must be emphasized to reduce the burden of NCDs.

Lipids play a vital role in human wellbeing. There is ample evidence that diets high in saturated and trans fats increase the risk of NCDs, whereas diets rich in unsaturated fatty acids reduce that risk (Nykiel et al., 2025). In 2003, in response to evidence showing adverse health effects of trans fat, the US Food and Drug Administration (US-FDA) proposed legislation to reduce trans fat. Subsequently, following the guidelines set forth by the US-FDA, many other countries also formulated their national policies to control the TFA content in their food supply (Umayangani et al., 2025)and as a result, they have virtually eliminated the TFA from their food supply. In Sri Lanka, initial steps were taken to establish legislation on TFA levels (not exceeding 2 g/100g of total fat) in Sri Lankan foods by the WHO (Country Office Sri Lanka) and the Ministry of Health (Lanerolle & de Lanerolle, 2020). As a consequence, the Ministry of Health, in consultation with the Food Advisory Committee, made a regulation under Section 32 of the Food Act, No. 26 of 1980 (The Food (Trans-Fat) Regulations, 2022), which shall come into operation with effect from January 01, 2026. requires that the amount of trans fat per 100 g or 100 mL be declared on the label of packaged food products, and it sets a maximum limit of 2% trans fat (excluding naturally occurring trans fat in animal fat) of the total fat content in foods intended for final consumers (Ministry of Health and Mass Media, 2025).

Bakery products play a crucial role in the daily diets of most people worldwide. Despite the popularity of bakery products as a convenient food, their nutritional quality is a major concern due to their lipid composition. Bakery fats such as margarine and shortening give bakery products unique texture and flavor. Most of the bakery fats currently used in Sri Lanka are manufactured using a conventional oil structuring technique called partial hydrogenation. The solid fats manufactured through this technique contain high levels of SFAs and industrially produced TFAs (Bihola et al., 2025). SFAs and industrially produced TFAs are given much attention due to their association with increasing the risk of several human ailments such as cardiovascular diseases, cancer, and type 2 diabetes. It is also reported that a 2% increase in energy intake from trans fat is associated with a 23% increase in cardiovascular risk (Singhal et al., 2023). The World Health Organization (WHO) has recommended that intake of saturated fats be less than 10% of total energy intake and that intake of trans fats be less than 1% of total energy intake (WHO, 2023).

The use of these solid fats in bakery products may eventually result in high SFA and TFA content in the final product. Therefore, bakery products available in the country should be analyzed for their fatty acid profiles to inform consumers about the nutritional quality and safety of these products. Only a limited number of studies have been reported in Sri Lanka on the fatty acid profiles of bakery products, with special emphasis on SFA and TFA contents. In this context, this study was designed to analyze the total fat content and fatty acid profiles of five different bakery products available in the Jaffna district. Findings of this study will be useful in raising awareness among people regarding the nutritional quality of bakery products and for policymakers in the health sector.

METHODOLOGY

Chemicals and reagents

All chemicals and authentic fatty acid standards for gas chromatography used in this study were purchased from Sigma Aldrich (St Louis, MO, USA). All chemicals used were of analytical grade.

Sampling

A total of 71 samples of commonly consumed bakery products, such as bread, buns, cakes, pastries, and doughnuts, were collected from 17 bakeries in the Jaffna district using non-probability sampling. Table 1 shows the sample collection from different places. The samples were brought to the laboratory on the same day of purchase to extract the fat. Each sample was analyzed separately.

Table 1: Locations of sample collection and types of samples collected

Location	Bakery Number	Samples Collected
Point Pedro	Bakery 1	Bread, Bun, Cake, Pastry
	Bakery 2	Bread, Bun, Cake
Karaveddi	Bakery 3	Bread, Bun, Cake, Pastry, Doughnut
	Bakery 4	Bread, Bun, Cake, Pastry, Doughnut
Valvettiturai	Bakery 5	Bread, Bun, Cake
Jaffna town	Bakery 6	Bread, Bun, Cake, Pastry, Doughnut
	Bakery 7	Bread, Bun, Cake, Pastry, Doughnut
	Bakery 8	Bread, Bun, Cake, Pastry
	Bakery 9	Bread, Bun, Cake, Pastry
	Bakery 10	Bread, Bun, Cake, Pastry
Kankesanthurai	Bakery 11	Bread, Bun, Cake, Pastry
Mallakam	Bakery 12	Bread, Bun, Cake, Pastry
Chunnakam	Bakery 13	Bread, Bun, Cake, Pastry
	Bakery 14	Bread, Bun, Pastry
Chavakacheri	Bakery 15	Bread, Bun, Cake
Atchuveli	Bakery 16	Bread, Bun, Cake
Kodikamam	Bakery 17	Bread, Bun, Cake

A total of 71 samples were collected (Breads (n=17), Buns (n=17), Cakes (n=16), Pastries (n=12), doughnuts (n=4) and bakery fats (n=5)). All samples were collected between mid of March to end of May 2021.

Extraction of fat

Fat from the samples was extracted by the solvent extraction method. The samples were pre-dried in a hot-air oven (Yamato, Japan) at 50±5 °C and ground into powder using a domestic blender. Fat was extracted from powdered samples by the solvent extraction method (Goldfisch method) (VELP Scientifica SER 148, Italy) using petroleum ether. After extraction, the solvent was evaporated using a rotatory evaporator (EYELA, N-1110, Japan) at 70 °C. The total fat content was calculated on a weight basis, and the extracted fat was used for fatty acid profile analysis.

Analysis of fatty acid profile by gas chromatography

Fatty Acid Methyl Esters (FAMEs) were prepared according to the WHO method (WHO, 2020) using BF_3-methanol. Prepared FAMEs were analyzed using a gas chromatograph (Agilent Technologies 7890B, USA) equipped with a Flame Ionization Detector and a fused-silica capillary column (100 m length, 0.25 mm internal diameter, 0.20 µm film as the stationary phase). Nitrogen was used as a carrier gas at a flow rate of 20 mL/min. FAMEs were injected (1 µL) at a split ratio of 30:1. The injector and detector temperatures were 260 ^{o}C. The initial column oven temperature was maintained at 140 ^{o}C for 5 mins, then increased to 240 ^{o}C at 4 ^{o}C/min, and maintained at that temperature for 10 mins. Identification of fatty acids was performed by comparing their retention times with the FAME standard (Supelco 37-component FAME mix and a mixture of *trans* isomers of linoleic acid).

Statistical analysis

All experiments were carried out in triplicate. The data were presented as the mean ± standard deviation in Microsoft Excel 2019. Analysis of Variance (ANOVA) was conducted using the Two-

Factor Completely Randomized Design in the Statistical Analysis System (SAS), version 6.0.10. Duncan's multiple range test was used to compare the treatment means among products at P<0.05.

RESULTS AND DISCUSSION

There were significant variations in total fat and fatty acid contents within and between bakery product types. According to the results shown in Table 2, the highest percentage of fat was observed in pastry and doughnut, and the lowest fat content was observed in bread. The mean total fat content across five categories of bakery products analyzed is as follows: pastry > doughnut > cake > bun > bread.

Table 2: Total fat content in different bakery products and bakery fats (g of fat/ 100 g product)

Sample	Bread	Bun	Cake	Pastry	Doughnut	Bakery fat
1	2.38±0.03^{bcd}	4.83±0.18^{ij}	25.33±0.10^{de}	28.57±0.13^{i}	37.17±0.10^{a}	84.01±2.31^{b}
2	2.20±0.06^{def}	7.41±0.04^{d}	26.09±0.35^{c}	29.93±0.16^{h}	35.87±0.01^{b}	69.56±1.22^{c}
3	2.32±0.03^{cd}	10.08±0.03^{b}	17.40±0.31^{j}	34.11±0.04^{d}	36.24±0.25^{b}	92.40±3.03^{a}
4	2.51±0.33^{bc}	4.96±0.20^{i}	26.07±0.18^{c}	32.25±0.10^{f}	31.66±0.31^{c}	62.40±1.50^{d}
5	1.13±0.07^{gh}	4.59±0.04^{j}	25.13±0.07^{e}	25.93±0.21^{j}		44.78±0.57^{e}
6	3.43±0.01^{a}	6.52±0.14^{f}	26.06±0.25^{c}	31.72±0.06^{g}		
7	3.26±0.03^{a}	8.61±0.13^{c}	22.48±0.14^{h}	25.43±0.18^{k}		
8	1.40±0.03^{g}	5.42±0.03^{h}	30.00±0.11^{a}	35.79±0.13^{c}		
9	1.22±0.08^{gh}	5.77±0.18^{g}	23.42±0.20^{g}	39.89±0.18^{a}		
10	2.02±0.06^{ef}	3.30±0.06^{k}	19.82±0.31^{i}	21.63±0.21^{l}		
11	2.25±0.07^{cde}	5.00±0.11^{i}	25.76±0.11^{cd}	39.51±0.18^{b}		
12	1.00±0.08^{h}	3.37±0.04^{k}	27.97±0.16^{b}	33.41±0.30^{e}		
13	2.38±0.08^{bcd}	6.95±0.07^{e}	25.80±0.28^{cd}			
14	1.93±0.04^{f}	7.17±0.04^{de}	23.60±0.11^{g}			
15	1.04±0.03^{h}	3.18±0.08^{k}	19.63±0.18^{i}			
16	2.36±0.28^{bcd}	3.26±0.20^{k}	24.06±0.23^{f}			
17	2.64±0.20^{b}	10.91±0.10^{a}				
Mean ± S.D. (Min-Max)	2.09±0.73 (1.00-3.43)	5.96±2.34 (3.18-10.91)	24.29±3.22 (17.40-30.00)	31.51±5.56 (21.63-39.83)	35.24±2.45 (31.66-37.17)	70.63±18.64 (44.78-92.40)

Means in each column followed by different superscript letters (a - l) are significantly different (P<0.05).

Fatty acids profile (mean values and ranges) of samples are shown in detail in Table 3. There were significant differences in the contents of different fatty acid types within and between the selected bakery products. Fatty acid composition is expressed as g of fatty acids per 100 g of total fat (mentioned as % hereafter).

Table 3: The mean value and minimum-maximum range of fatty acid composition of bread, bun, cake, pastry, doughnut, and bakery fat

Fatty acids	Bread	Bun	Cake	Pastry	Doughnut	Bakery fat
Caproic acid (C6:0)	0.09±0.12 (0.00-0.63)	0.07±0.27 (0.00-0.69)	-	-	0.02±0.00 (0.00-0.09)	0.07±0.00 (0.00-0.35)
Caprylic acid (C8:0)	3.05±2.14 (0.18-6.51)	2.24±1.09 (0.17-4.14)	1.99±1.46 (0.26-6.98)	0.78±0.64 (0.25-1.92)	0.70±0.27 (0.41-1.01)	1.47±1.94 (0.04-4.16)
Capric acid (C10:0)	2.30±1.72 (0.16-5.31)	1.75±0.88 (0.18-3.19)	1.60±1.14 (0.23-5.45)	0.61±0.49 (0.22-1.49)	0.56±0.24 (0.27-0.79)	1.17±1.57 (0.00-3.27)
Undecylenic acid (C11:0)	0.09±0.17 (0.00-0.71)	0.06±0.03 (0.00-0.13)	0.02±0.01 (0.00-0.06)	0.04±0.01 (0.00-0.06)	0.04±0.04 (0.00-0.10)	0.02±0.01 (0.00-0.05)
Lauric acid (C12:0)	19.53±12.65 (1.61-40.22)	13.77±6.02 (1.47-26.10)	12.65±5.15 (1.85-19.56)	5.46±4.55 (2.02-14.07)	4.83±1.93 (2.55-6.67)	10.12±12.80 (0.40-26.48)
Myristic acid (C14:0)	8.02±5.13 (1.39-16.90)	6.38±2.32 (1.15-10.79)	6.25±3.31 (0.00-17.31)	3.18±1.88 (1.78-6.89)	2.70±0.67 (1.87-3.35)	4.91±4.91 (1.22-11.44)
Palmitic acid (C16:0)	32.12±10.78 (15.61-47.34)	35.56±5.08 (24.41-46.24)	38.58±7.90 (29.31-58.65)	44.69±3.96 (36.16-48.55)	39.55±2.69 (36.17-42.37)	45.70±13.92 (29.27-61.17)
Margaric acid (C17:0)	0.01±0.00 (0.00-0.18)	-	-	-	-	-
Stearic acid (C18:0)	0.07±0.05 (0.00-0.82)	-	-	-	-	-
Total SFA	**65.28±11.75 (46.15-84.13)**	**59.83±5.77 (46.93-68.90)**	**61.09±7.39 (53.97-85.34)**	**54.76±5.28 (50.59-69.78)**	**48.40±3.63 (46.15-53.75)**	**63.46±8.51 (55.10-74.97)**
Palmitoleic acid (C16:1)	0.22±0.34 (0.00-1.14)	0.03±0.00 (0.00-0.44)	-	-	-	-
Cis-10 Heptadecenoic acid (C17:1)	0.12±0.26 (0.00-0.70)	0.01±0.00 (0.00-0.14)	-	-	0.02±0.00 (0.00-0.07)	-
Oleic acid (C18:1)	22.16±8.32 (9.43-34.56)	28.09±5.69 (20.33-44.19)	28.86±5.44 (10.67-36.77)	30.78±2.89 (22.15-33.20)	37.59±3.82 (32.88-41.37)	28.24±8.22 (16.84-38.02)

Total MUFA	**22.50±8.37 (10.19-34.85)**	**28.13±5.69 (20.33-44.19)**	**28.86±5.44 (10.67-36.77)**	**30.78±2.89 (22.15-33.20)**	**37.61±3.85 (32.88-41.44)**	**28.24±8.22 (16.84-38.02)**
Linoleic acid (C18:2)	11.72±5.15 (4.48-23.02)	10.04±2.61 (6.04-14.81)	8.58±2.58 (3.99-15.49)	6.63±1.69 (3.81-8.23)	11.91±2.20 (9.11-13.92)	5.97±1.60 (3.34-7.45)
Total PUFA	**11.72±5.15 (4.48-23.02)**	**10.04±2.61 (6.04-14.81)**	**8.58±2.58 (3.99-15.49)**	**6.63±1.69 (3.81-8.23)**	**11.91±2.20 (9.11-13.92)**	**5.97±1.60 (3.34-7.45)**
Total UFA	**34.23±11.13 (15.87-48.90)**	**38.17±6.16 (28.64-53.07)**	**37.44±6.71 (14.66-43.84)**	**37.41±3.92 (27.45-41.43)**	**49.50±3.40 (46.26-53.83)**	**34.22±9.60 (20.18-44.91)**
Elaidic acid (C18:1 *trans*)	0.17±0.00 (0.00-2.96)	1.57±1.47 (0.00-6.13)	1.18±2.06 (0.00-6.19)	7.83±1.67 (2.77-8.95)	2.10±1.27 (0.00-5.10)	2.32±1.70 (0.00-4.89)
Linolelaidic acid (C18:2 *trans* 9,12)	0.32±0.37 (0.00-1.99)	0.43±1.23 (0.00-4.51)	0.29±0.80 (0.00-2.86)	-	-	-
Total TFA	**0.49±1.26 (0.00-4.95)**	**2.00±2.36 (0.00-6.13)**	**1.47±2.28 (0.00-6.19)**	**7.83±1.67 (2.77-8.95)**	**2.10±1.27 (0.00-5.10)**	**2.32±1.70 (0.00-4.89)**

All bakery products predominantly consisted of SFAs. Some products consisted of TFAs such as elaidic acid (C18:1 *trans*) and *trans* isomers of linoleic acid. All bakery products consisted of palmitic acid as the predominant SFA. However, some (6 out of 17) bread samples showed lauric acid as the predominant fatty acid (up to 40.22±0.05%) and myristic acid as the second-most abundant (>16%) fatty acid (e.g., samples 2 and 11).

Average SFA content of breads was 65.28±11.75 g/100 g fatty acids. However, the contribution of bread as a source of SFA is very low due to its lower total fat content (2.09±0.73 g/100 g bread). Bun samples are also dominated by palmitic acid with an average of 35.56±5.08% (24.41- 46.24%). That is, bun samples consisted of more palmitic acid compared to bread samples. Lauric acid also contributes a considerable amount of SFA with an average of 13.77±6.02% (1.47- 26.10%). Average SFA was 59.83±5.77% (46.93-68.90%). Cake samples are also dominated by palmitic acid and lauric acid; however, the contribution of lauric acid to SFA content is less compared to bread and bun. Average SFA was 61.09±7.39% (53.97- 85.34%). Both pastry and doughnut samples are dominated by palmitic acid, with average values of 44.69±3.96% and 39.55±2.69%, respectively. Average SFA content in the pastry sample was 54.76±5.28% (50.59-69.78%). A serving of 100 g pastry will contribute nearly 17.25 g SFA (average fat content of pastry is 31.51±5.56 g/100 g). Average SFA in the doughnut sample was 48.40±3.63%, ranging from 46.15 to 53.75%.

In the bakery fats, palmitic acid was detected as the major SFA. Average SFA of these bakery fats was 63.46±8.51% (55.10- 74.97%). The total SFA content of samples ranged from 46.15-85.34 g/100 g of fat. The mean SFA content as expressed in g/100 g of bread, bun, cake, pastry, and doughnuts was 1.36, 3.57, 14.83, 17.25, and 17.06, respectively. Some bakery samples had palmitic acid and SFA percentages that were nearly similar to those reported for bakery fats.

Oleic acid (C18:1) was the predominant MUFA obtained in all bakery products. However, palmitoleic acid (C16:1) and *cis*-10 heptadecenoic acid (C17:1) were obtained in some bread, bun, and doughnut samples. According to the results (for a 100 g serving of the sample), the unsaturated fatty acid content across five categories of bakery products analyzed was as follows: doughnut > pastry > cake > bun > bread.

Elaidic acid (C18:1 *trans*) and linolelaidic acid (C18:2 *trans* 9,12) were detected as TFAs in the samples. However, elaidic acid (C18:1 *trans*) was the predominant TFA obtained in all categories. Some samples were not detected for any TFAs. All pastry samples contained TFAs, whereas 17.64%, 47.05%, 37.5%, 50%, and 80% of bread, bun, cake, doughnut, and bakery fats, respectively, were detected with TFAs. TFA content (in range) of bread, bun, cake pastry, and doughnuts as expressed in g/100 g of fat were 0.00-4.95, 0.00-6.13, 0.00-6.19, 2.77-8.95, and 0.00-5.10, respectively. Pastry is the only category detected with TFA in all samples. Therefore, in other samples, calculating the average TFA by considering the total number of samples analyzed may underestimate the TFA content; that is, the average TFA will be much lower than the actual value. For instance, among the 17 bread samples, only 3 contained TFA. To avoid this, we calculated the average TFA content by considering the number of samples detected with TFA in each category. Accordingly, the average TFA content per 100 g of the sample was 2.47 g for pastries, 1.54 g for doughnuts, 1.03 g for cakes, 0.28 g for buns, and 0.08 g for breads. According to the results, the TFA content (per 100 g of serving) across five categories of bakery products analyzed was as follows: pastry > doughnut > cake > bun > bread. TFA content of these bakery products ranged from 0.08 g to 2.47 g/100 g product.

Bakery fats (margarine and shortening) consisted of elaidic acid (C18:1 *trans*) as the only TFA. Average TFA was 2.32±1.70%, ranging from 0.00 to 4.89%. One bakery fat contained no TFA.

There were significant differences in total fat content among samples of each type ($P<0.05$). This could be because different bakers use different types of fat in varying amounts. A study conducted in Sri Lanka (Wasana et al., 2021) demonstrated that bakery products available in markets in the Colombo district contained total fat ranging from 4.93±0.03 to 14.22±0.1%, which is lower than the values reported in the present study.

Fatty acid percentages of bakery fats are almost similar to most bakery samples. However, some samples contained higher TFA levels than those present in the bakery fats and also the trans isomers of linoleic acid, which were not detected in any of the bakery fats. This could be due to the conversion of *cis* isomers into *trans* isomers during high-temperature processing (Mavlanov et al., 2025). Therefore, considering baking temperature and the optimal use of bakery fats would help control TFA levels in baked products.

Although most samples had palmitic acid as the predominant SFA, some had lauric or myristic acid as the predominant SFA. The presence of these medium-chain fatty acids in some samples could be due to bakery fats produced from coconut oil, which contains lauric acid and myristic acid as major SFAs (Mavlanov et al., 2025). A similar observation of high proportions of lauric acid (53.53%) and myristic acid (21.17%) was reported in coconut bread (AlJuhaimi et al., 2024).

According to WHO, the SFA consumption should be less than 10% of a person's total energy intake (WHO, 2023). According to the findings of this study, except for breads and buns, some samples from other categories may exceed the WHO critical limit (based on serving size). A previous study reported that pastry samples sold in Sri Lanka contained SFA ranging from 5.19% to 10.32% (Dassanayake et al., 2024). These values are lower than those reported for the pastry samples in the present study.

TFAs are an important group of fatty acids of special concern due to their associated adverse health effects. WHO recommends that TFA intake should be less than 1% of total energy intake (WHO, 2023). Accordingly, TFAs need to be reduced to less than 2% of total fat in oils. In other words, consumption of no more than 2.2 g of TFAs per day for an adult consuming 2000 kcal per day is recommended (WHO, 2021). About 39.39% of the samples analyzed in this study had TFA levels significantly above the critical limit. These findings indicate that a significant proportion of the samples analyzed in this study are unsafe to consume due to their TFA content. A few earlier studies conducted in different parts of Sri Lanka have reported varying results for the TFA content of bakery products. A previous study reported that bakery products available in the Colombo district contained TFAs ranging from 20.76±0.239 to 39.98±0.377%. A landscape study conducted in the country has demonstrated that bread samples collected from different parts of the country had TFA levels ranging from 0 to 1.8 g/100 g of fat (Lanerolle & de Lanerolle, 2020). These variations could be due to the type and amount of solid fat used by the bakers.

Studies reported in other countries also demonstrated varying fatty acid compositions, and some findings agree with those reported in this study. For example, bakery products in Brazil are reported to contain 0.1-6.1 g/100 g of TFA and 1.1-16.9 g/100 g of SFA, with total fat content of 7.0-33.3 g/100 g (Aued-Pimentel & Kus-Yamashita, 2021). A recent study conducted in Slovenia reported that the breads contained 0.12±0.17 TFAs, corresponding to 2 g/100 g of bread (Kušar et al., 2021), which is also similar to the values reported in the present study. A study in the Portuguese market reported TFA content of pastries as 1.96% (0.07–8.47) (Costa *et al*., 2016).A study conducted in the Spanish market reported that TFA content in pastries ranged from 0.11% to 0.30% (Zamora-Ledezma et al., 2025). However, studies have reported much higher TFA contents in bakery products than in the present study. A study from Iran reported TFA content of 0.44±0.56% in cakes (Hadian & Khaneghah, 2022). Another study conducted in the Slovenian market reported TFA levels ranging from 0.10% to 1.71% in bread (Mencin et al., 2021). Comparatively, the TFA content in the bakery products analyzed in the present study is lower than that in bakery products sold in some other countries. However, many countries have successfully reduced TFA levels in their food supply (Al-Jawaldeh et al., 2021) due to legislation on TFA content in foods. According to WHO, a total of 53 countries had best-practice policies in place to tackle industrial trans-fat in food (WHO, 2024). In Sri Lanka, even though legislation related to TFA levels in foods will be implemented in the near future, efforts should engage food manufacturers, and reformulating products to reduce or eliminate saturated and trans fats may take considerable time.

CONCLUSION

Although there was high variability in the fatty acid content of bakery products from bakeries, the present study indicates that bakery products sold in Jaffna markets contain higher levels of SFAs and TFAs than recommended levels. These findings strongly suggest the need to implement legislation on TFA content, reformulate products, or use alternative bakery fats with reduced SFA and TFA to avoid adverse effects on human health. Proper labeling and public awareness of the health effects of consuming different types of fats and bakery products will help reduce the impact on health. An estimate of dietary intake, based on a suitable technique for assessing food consumption patterns, is necessary to determine the daily consumption of SFA and TFA among Sri Lankans.

Declaration of conflict of interest

The authors declare no conflicts of interest.

Funding information

The funding from the University Research Grant (URG/2019/SEIT/05) of the University of Jaffna, Sri Lanka is greatly appreciated.

REFERENCES

[1] Al-Jawaldeh, A., Taktouk, M., Chatila, A., Naalbandian, S., Abdollahi, Z., Ajlan, B., Al Hamad, N., Alkhalaf, M. M., Almamary, S., Alobaid, R., Alyafei, S. A., Azizi, M. H., Baqadir, N. M., Barham, R., Binsunaid, F. F., El Ammari, L., El Ati, J., Hoteit, M., Massad, H., … Nasreddine, L. (2021). A Systematic Review of Trans Fat Reduction Initiatives in the Eastern Mediterranean Region. Frontiers in Nutrition, 8(November). https://doi.org/10.3389/fnut.2021.771492

[2] AlJuhaimi, F., Ahmed, I. A. M., Özcan, M. M., & Albakry, Z. (2024). Influence of coconut pulp on bioactive properties, fatty acids, phenolic compounds, nutrients and sensory evaluation of wheat flour bread. International Journal of Food Science & Technology, 59(6), 4020–4029. https://doi.org/https://doi.org/10.1111/ijfs.17157

[3] Aued-Pimentel, S., & Kus-Yamashita, M. M. (2021). Analysis of the fat profile of industrialized food in Brazil with emphasis on trans-fatty acids. Journal of Food Composition and Analysis, 97(January), 103799. https://doi.org/10.1016/j.jfca.2020.103799

[4] Bihola, A., Chaudhary, M. B., Bumbadiya, M. R., Suvera, P., & Adil, S. (2025). Technological innovations in margarine production: Current trends and future perspectives on trans-fat removal and saturated fat replacement. Comprehensive Reviews in Food Science and Food Safety, 24(1), e70088. https://doi.org/https://doi.org/10.1111/1541-4337.70088

[5] Cesare, M. D., Bixby, H., Gaziano, T., Hadeed, L., Kabudula, C., McGhie, D. V., Mwangi, J., Pervan, B., Perel, P., Piñeiro, D., Taylor, S., & Pinto, F. (2023). World Heart Report 2023: Confronting the World’s Number One Killer. World Heart Federation, 1–52. https://world-heart-federation.org/wp-content/uploads/World-Heart-Report-2023.pdf

[6] Costa, N., Cruz, R., Graça, P., Breda, J., & Casal, S. (2016). Trans fatty acids in the Portuguese food market. Food Control, 64, 128-134. doi: 10.1016/j.foodcont.2015.12.010

[7] Dassanayake, R., Somasiri, S., Mahanama, K., & Premakumara, S. (2024). Fatty Acid and Sterol Profiles of Commonly Available Street Foods in Sri Lanka: Comparison to Other Countries in the Asian Region. Journal of Food Processing and Preservation, 2024(Cvd). https://doi.org/10.1155/2024/7350661

[8] Hadian, Z., & Khaneghah, A. M. (2022). Sugar, fat, saturated and trans fatty acid contents in Iranian cereal-based baked products. Food Science and Technology (Brazil), 42, 1–11. https://doi.org/10.1590/fst.26724

[9] Kušar, A., Hribar, M., Lavriša, Ž., Zupanič, N., Pivk Kupirovič, U., Hristov, H., Abramovič, H., Vidrih, R., Zlatić, E., Kokalj, D., Piskernik, S., Mencin, M., Peče, P., Blaznik, U., Žmitek, K., & Pravst, I. (2021). Assessment of trans-fatty acid content in a sample of foods from the Slovenian food supply using a sales-weighting approach. Public Health Nutrition, 24(1), 12–21. https://doi.org/10.1017/S1368980020001949

[10] Lanerolle, P., & de Lanerolle D. M. (2020). Landscape analysis for trans fat limits for Sri Lanka: A synthesis report and policy brief. World Health Organization. Country Office for Sri-Lanka.

[11] Mavlanov, U., Czaja, T. P., Nuriddinov, S., Dalimova, D., Dragsted, L. O., Engelsen, S. B., & Khakimov, B. (2025). The effects of industrial processing and home cooking practices on trans-fatty acid profiles of vegetable oils. Food Chemistry, 469(August 2024). https://doi.org/10.1016/j.foodchem.2024.142571

[12] Mencin, M., Abramovič, H., Zlatić, E., Demšar, L., Piskernik, S., Schreiner, M., Žmitek, K., Kušar, A., Pravst, I., & Vidrih, R. (2021). Content of trans-fatty acid isomers in bakery products on the Slovenian market. LWT, 143(August 2020). https://doi.org/10.1016/j.lwt.2021.111095

[13] Ministry of Health and Mass Media (2025). Food (Trans-Fat) Regulations, 2022 (as amended). The Gazette of the Democratic Socialist Republic of Sri Lanka, Extraordinary, No. 2443/07. Available at: chrome-

extension://efaidnbmnnnibpcajpcglclefindmkaj/https://eohfs.health.gov.lk/food/images/English_The_Food_trans-Fat_Regulation_2022.pdf
[14] Ministry of Health Sri Lanka. (2024). Annual Health Bulletin 2022-2023. 1–23.
[15] Nykiel, S., Misiuk, J., Kopeć, K., Bartoszek, A., Adamiuk, J., Marut, A., Biskup, M., Skuba, A., Załuska, K., & Świdniak, A. (2025). The Dietary Fats: A Comprehensive Study about the Influence of Different Types of Fats on General Health and Developing Diseases. Quality in Sport, 40, 58799. https://doi.org/10.12775/qs.2025.40.58799
[16] Singhal, P., Osmani, S., & Taduru, A. S. (2023). Trans Fats and their Effects on Various Diseases: A Review. Acta Scientific Nutritional Health, 7(5), 45–52. https://doi.org/10.31080/asnh.2023.07.1233
[17] Umayangani, S., De Silva, I., Munasinghe, D., Deshika, C., Chandrapala, J., & Silva, M. (2025). Elimination of Trans Fatty Acids from Foods Using Novel Technologies. Food Reviews International, 1–29. https://doi.org/10.1080/87559129.2025.2502439
[18] Varghese, C., Prem, A., Nongkynrih, B., Chattu, V. K., & Mikkelsen, B. (2025). Fourth UNHLM on noncommunicable diseases 2025: An opportunity to bridge the transcending priorities for impact in global south. PLOS Global Public Health, 5(3), 8–11. https://doi.org/10.1371/journal.pgph.0004287
[19] Wasana, M. L. D., De Silva, A., Gunawardana, N., Illeperuma, D. C. K., Weerasinghe, W. M. P. B., Weerathunga, W. M. D. C., Ekanayake, S., & Madhujith, T. (2021). Study on Trans Fat Content of Selected Foods Commercially Available in Colombo District of Sri Lanka. Tropical Agricultural Research, 32(4), 471. https://doi.org/10.4038/tar.v32i4.8515
[20] WHO. (2020). Global protocol for measuring fatty acid profiles of foods, with emphasis on monitoring trans-fatty acids originating from partially hydrogenated oils. In WHO laboratory protocol. World Health Organization.
[21] WHO. (2021). REPLACE trans fat: an action package to eliminate industrially produced trans-fatty acids. World Health Organization, 1–8. https://www.who.int/teams/nutrition-and-food-safety/replace-trans-fat
[22] WHO. (2023). Saturated Fatty Acids. In Encyclopedia of Immunotoxicology: Second Edition. https://doi.org/10.1007/978-3-642-54596-2_201315
[23] WHO. (2024). Countdown to 2023: WHO 5-year milestone report on global trans fat elimination 2023 (Vol. 5, Issue May). https://www.who.int/publications/i/item/9789240089549%0Ahttps://www.who.int/teams/nutrition-and-food-safety/replace-trans-fat
[24] WHO. (2025). Monitoring health for the SDGs. The global health observatory. https://www.who.int/data/gho/data/themes/world-health-statistics
[25] Zamora-Ledezma, C., Martínez-Hernandez, J. M., Elango, J., Garcia-Garrido, J., Morillas-Ruiz, J. M., Díaz-Cruces, E., Miró-Colmenárez, P. J., & Zamora-Ledezma, E. (2025). Trans Fats in Spanish Pastries and Their Influence on Mesenchymal Stem Cell Behavior In Vitro and Related Health Risks. Foods, 14(13). https://doi.org/10.3390/foods14132247

Knowledge and awareness of medicinal values of selected traditional rice varieties among villagers in Wellawaya, Sri Lanka: A pilot study

Running Title: Awareness of Traditional Rice Medicinal Values in Wellawaya

R.M.B.N Dilrukshi, D.A.L Munasinghe *, Y.S.G Wimalasiri

Faculty of Indigenous Medicine, University of Colombo

ABSTRACT

Traditional rice varieties in Sri Lanka possess significant cultural, nutritional, and medicinal value. However, modernization of agriculture and replacement with high-yielding varieties has contributed to declining cultivation and erosion of indigenous knowledge systems. This pilot study aimed to assess the knowledge and awareness of medicinal values of selected traditional rice varieties among villagers in Wellawaya, Sri Lanka. A community-based cross-sectional descriptive survey was conducted among 30 participants selected through systematic random sampling. Data were collected using a pre-tested structured questionnaire through face-to-face interviews. Descriptive statistics were used to summarize demographic characteristics and awareness levels, while chi-square tests were applied as exploratory analyses to examine associations between demographic variables and knowledge levels. Findings revealed moderate general awareness of traditional rice varieties, with higher recognition of Suwadel, Kalu Heenati, and Maa Wee. However, knowledge of specific medicinal properties was limited. Although older participants and those engaged in agriculture demonstrated relatively higher knowledge levels, no statistically significant associations were observed ($p > 0.05$), likely due to the limited sample size and reduced statistical power inherent in pilot studies. The study indicates a gradual erosion of community-level knowledge regarding medicinal applications of traditional rice. These findings provide preliminary evidence to inform larger-scale studies and support policy initiatives aimed at preserving indigenous knowledge and promoting traditional rice varieties for nutritional and health benefits in Sri Lanka.

Keywords: Community awareness, Indigenous knowledge, Medicinal properties, Pilot study, Sri Lanka

----

* munasinghe@fim.cmb.ac.lk

INTRODUCTION

Rice (*Oryza sativa* L.) is the staple food of Sri Lanka and forms the dietary foundation of the population. Historically, Sri Lanka cultivated a wide diversity of indigenous rice varieties adapted to different agro-ecological zones and cultural practices. These traditional varieties were not only food sources but also held cultural and medicinal significance, particularly within indigenous Ayurvedic systems.

Traditional rice varieties such as Suwadel, Kalu Heenati, Pachchaperumal, and Maa-Wee are recognized for their superior nutritional composition, including higher levels of dietary fibre, phenolic compounds, antioxidants, and micronutrients. These bioactive components have been associated with improved glycaemic control and reduced oxidative stress (Abeysekera et al., 2017; Ranaweera et al., 2014).

Non communicable diseases (NCDs), including diabetes, cardiovascular diseases, and obesity, are increasing in Sri Lanka and globally. Dietary interventions using functional foods such as traditional rice varieties have been identified as a potential preventive strategy (World Health Organization [WHO], 2022). Additionally, agricultural biodiversity plays a critical role in food security and sustainable development (Toledo & Burlingame, 2006).

Despite scientific recognition of their nutritional value, indigenous knowledge regarding the medicinal uses of traditional rice varieties is declining. Modern agricultural practices and the dominance of high-yielding rice varieties have contributed to erosion of biodiversity and intergenerational knowledge loss (Biodiversity Secretariat, 2016). However, limited empirical research has assessed community level awareness of these medicinal properties.

Therefore, this pilot study aimed to assess knowledge and awareness of medicinal values of selected traditional rice varieties among villagers in Wellawaya, Sri Lanka.

OBJECTIVES

General Objective

To assess community-level knowledge and awareness of medicinal values of selected traditional rice varieties in Wellawaya, Sri Lanka.

Specific Objectives

To evaluate awareness of selected traditional rice varieties

To assess knowledge of their medicinal properties

To determine associations between demographic characteristics and knowledge levels

LITERATURE REVIEW

Sri Lanka has historically maintained a rich diversity of rice germplasm, with over 2,000 traditional rice varieties reported to have been cultivated across different agro-ecological zones (Biodiversity Secretariat, 2016). These varieties have long been valued not only for their adaptability and resilience but also for their nutritional and therapeutic significance within indigenous medical systems.

A growing body of scientific literature has provided evidence supporting the enhanced nutritional properties of traditional rice varieties. Abeysekera et al. (2017) demonstrated that several Sri Lankan traditional red rice varieties exhibit higher antioxidant activity in bran extracts compared to modern improved varieties. Similarly, Ranaweera et al. (2014) reported that indigenous rice varieties possess significantly higher phenolic content and antioxidant capacity, suggesting their potential role in reducing oxidative stress and associated chronic diseases.

Further supporting these findings, Gunathilake et al. (2024) identified that traditional varieties such as Suwadel and Pachchaperumal contain higher levels of dietary fibre and essential micronutrients. These nutritional characteristics are increasingly associated with improved glycaemic regulation and metabolic health outcomes, particularly in populations affected by non-communicable diseases.

On a broader scale, biodiversity has been recognised as a critical determinant of nutritional security and sustainable food systems. Toledo and Burlingame (2006) emphasised the interrelationship between biodiversity conservation and human nutrition, highlighting the importance of maintaining traditional food systems for longterm health and sustainability.

Despite this growing scientific evidence at the biochemical and nutritional level, most existing studies have focused on laboratory-based analyses of rice composition. Relatively little attention has been given to understanding how such nutritional and medicinal knowledge is perceived, retained, and transmitted within rural communities. In particular, there is a lack of empirical evidence on community awareness of the medicinal values of traditional rice varieties in Sri Lanka.

This gap is significant because the sustainability of traditional rice conservation efforts depends not only on agronomic and biochemical validation but also on community knowledge and cultural transmission. Therefore, assessing public awareness is essential for linking scientific evidence with indigenous knowledge systems and for informing culturally appropriate agricultural and public health interventions.

METHODOLOGY

Study Design

A community-based cross-sectional descriptive study design was employed.

Study Area

The study was conducted in Wellawaya, Monaragala District, Uva Province, Sri Lanka.

Sample Size

The sample size for the main study was estimated using the standard prevalence formula (Naing et al., 2006):

$$N = Z^2P(1-P)/D^2$$

Where Z = 1.65 (90% confidence level), P = 0.5 (assumed maximum variability), and D = 0.047 (margin of error).

The calculated sample size for the main study was 300. As this investigation was designed as a pilot study, 10% of the calculated sample size (n = 30) was selected in accordance with established guidance for pilot research, which recommends using approximately 10% of the main study sample to assess feasibility, instrument clarity, and preliminary trends (Hazzi & Maldaon, 2015). The use of a 90% confidence level was considered appropriate for this exploratory pilot study aimed at generating preliminary evidence rather than making population-level generalisations.

Sampling Technique

Systematic random sampling was used to select households. One eligible participant per household was recruited.

Inclusion Criteria
• Individuals aged 18–70 years
• Permanent residents of Wellawaya
• Willingness to participate and provide informed consent

Exclusion Criteria
• Individuals below 18 or above 70 years
• Individuals unwilling to participate
• Individuals with physical or psychological conditions that could impair participation

Data Collection Instrument

Data were collected using a pre-tested structured questionnaire developed based on relevant literature. Content validity was assessed by experts in Indigenous Medicine. The questionnaire consisted of three sections: demographic characteristics, awareness of traditional rice varieties, and knowledge of medicinal properties.

The internal consistency reliability of the knowledge assessment section was evaluated using Cronbach's alpha (α=0.80).

Data Collection Procedure

Face to face interviews were conducted from June to August 2025. Written informed consent was obtained from all participants prior to data collection.

Ethical Considerations

Ethical approval was obtained from the Ethical Review Committee of the Faculty of Indigenous Medicine, University of Colombo (ERC UG 25/358). Confidentiality and anonymity of participants were strictly maintained throughout the study.

Statistical Analysis

Data were analysed using SPSS version 26. Descriptive statistics were used to summarise demographic characteristics and awareness levels. Knowledge scores were computed based on correct responses and categorised into low and moderate levels using predetermined cutoff values based on score distribution.

Pearson's chi-square test was used as an exploratory analysis to examine associations between demographic variables and knowledge levels. Statistical significance was set at $p < 0.05$. Given the small pilot study sample size, results of inferential tests were interpreted cautiously due to limited statistical power.

RESULTS AND DISCUSSION

Demographic Characteristics

Among the 30 participants, 40% were aged between 61–70 years, indicating a relatively older sample population. Males constituted 63% of the respondents. Nearly half of the participants had education up to the Ordinary Level, while 43.33% were engaged in farming activities.

Awareness of Traditional Rice Varieties

All respondents reported familiarity with at least one traditional rice variety, indicating that these rice types remain culturally recognised within the study population. Suwadel (73.33%), Heenati (70%), and Maa-Wee (53.33%) were the most commonly identified varieties, suggesting sustained cultural visibility of specific traditional rice types.

Knowledge of Medicinal Properties

Although general awareness of traditional rice varieties was relatively high, detailed knowledge of their medicinal properties was limited. Heenati (63.33%) was most frequently associated with therapeutic benefits, whereas other varieties were inconsistently linked to specific health effects. This indicates that while recognition persists, depth of knowledge regarding medicinal applications is fragmented at the community level.

Inferential Analysis

Chi-square analysis revealed no statistically significant association between knowledge levels and age ($p = 0.471$), gender ($p = 0.717$), education ($p = 0.509$), or occupation ($p = 0.205$). These findings suggest that demographic variables were not strong predictors of knowledge within this sample. However, given the small sample size, these results should be interpreted cautiously as the study had limited statistical power to detect significant associations.

Discussion

The findings of this study indicate a clear distinction between cultural recognition of traditional rice varieties and detailed knowledge of their medicinal properties. While awareness remains relatively high, particularly for varieties such as Suwadel and Heenati, in-depth understanding of their health-related benefits appears to be diminishing.

This pattern aligns with concerns regarding the erosion of indigenous knowledge systems in Sri Lanka, particularly in rural communities undergoing agricultural transition (Biodiversity Secretariat, 2016). The observed higher awareness among older and farming participants, although not statistically significant, may reflect experiential knowledge acquisition and intergenerational transmission, which are key mechanisms in sustaining traditional ecological knowledge.

Similar trends have been reported in other contexts where modernization of agriculture has led to reduced reliance on traditional crops and associated knowledge systems. The weakening of such knowledge transmission may reduce community engagement with nutritionally beneficial traditional foods, despite increasing global recognition of functional foods in preventing non-communicable diseases (World Health Organization, 2022).

From a public health and agricultural perspective, these findings highlight the need for integrated awareness programmes that connect scientific evidence on nutritional benefits with community-level knowledge systems. Strengthening agricultural extension services and incorporating traditional rice knowledge into local education initiatives may contribute to both biodiversity conservation and improved dietary practices.

CONCLUSION

This pilot study demonstrated that villagers in Wellawaya possess moderate awareness of traditional rice varieties but limited detailed knowledge of their medicinal properties. No

statistically significant associations were observed between demographic factors and knowledge levels, likely due to the limited sample size and exploratory nature of the study.
The findings suggest a gradual decline in detailed indigenous knowledge related to traditional rice varieties. Strengthening documentation, community education, and agricultural extension programmes is recommended to preserve this knowledge and promote its integration into nutrition and public health strategies. Further large-scale studies are required to confirm these preliminary findings and support policy development in this area.

REFERENCES

[1] Abeysekera, W. K. S. M., Arachchige, S. P. G., Ratnasooriya, W. D., Chandrasekharan, N. V., & Bentota, A. P. (2017). Physicochemical and nutritional properties of twenty-three traditional rice (Oryza sativa L.) varieties of Sri Lanka. Journal of Coastal Life Medicine, 5(8), 343–349.

[2] Biodiversity Secretariat. (2016). National biodiversity strategic action plan of Sri Lanka 2016–2022. Ministry of Mahaweli Development and Environment.

[3] Gunathilake, K. D. P. P., Ranaweera, K. K. D. S., & Rupasinghe, H. P. V. (2024). Nutritional and antioxidant properties of traditional rice varieties of Sri Lanka. Journal of Food Composition and Analysis, 115, 104944.

[4] Hazzi, O. A., & Maldaon, I. (2015). A pilot study: Vital methodological issues. Business: Theory and Practice, 16(1), 53–62.

[5] Juliano, B. O. (1993). Rice in human nutrition. Food and Agriculture Organization of the United Nations.

[6] Naing, L., Winn, T., & Rusli, B. N. (2006). Practical issues in calculating sample size for prevalence studies. Archives of Orofacial Sciences, 1, 9–14.

[7] Ranaweera, K. K. D. S., Gunathilake, K. D. P. P., & Rupasinghe, H. P. V. (2014). Nutritional and antioxidant properties of selected Sri Lankan traditional rice varieties. International Journal of Food Science & Technology, 49(2), 471–478.

[8] Toledo, A., & Burlingame, B. (2006). Biodiversity and nutrition: A common path toward global food security and sustainable development. Journal of Food Composition and Analysis, 19(6–7), 477–483.

[9] World Health Organization. (2022). Noncommunicable diseases country profiles 2022. WHO Press.

Controlled Sulfur Incorporation in SILAR-Deposited CdS Quantum Dots for Suppression of Interfacial Recombination in TiO_2 Quantum Dot-Sensitized Solar Cells

N.F. Ajward*, J.V.P. Fernando and V.P.S. Perera

Department of Physics, The Open University of Sri Lanka, Nawala, Nugegoda

ABSTRACT

Quantum dot-sensitized solar cells (QDSSCs) are limited by severe interfacial recombination and inefficient electron transport at the TiO_2/CdS junction. In this work, the interfacial charge dynamics were controlled by regulating sulfur availability during successive ionic layer adsorption and reaction (SILAR) growth of CdS quantum dots on mesoporous TiO_2 photoanodes. Sulfur was introduced in controlled molar ratios relative to the Cd^{2+} precursor to modify defect density and band alignment.

An optimum sulfur level produced a marked improvement in photovoltaic performance, where power conversion efficiency increased from 0.262% (undoped CdS) to 0.519%, accompanied by higher photocurrent density and open-circuit voltage. Electrochemical impedance analysis showed a strong increase in recombination resistance and a prolonged electron lifetime (0.017 s → 0.159 s), while Mott–Schottky measurements revealed a positive flat-band shift (−0.747 V → −0.588 V vs Ag/AgCl), indicating improved interfacial energetics. The enhancement originates from sulfur-induced passivation of surface trap states in CdS, which suppresses back electron transfer to the electrolyte and facilitates forward electron transport through the TiO_2 network. Consequently, performance enhancement is dominated by interfacial recombination suppression.

These results demonstrate that tuning sulfur incorporation during CdS growth provides a simple and scalable strategy to engineer interfacial charge transport and improve the efficiency and stability of TiO_2/CdS QDSSCs.

Keywords: Quantum Dot-Sensitized Solar Cells (QDSSCs), Sulfur Doping, Cadmium Sulfide, SILAR, Photovoltaic Performance

----

* nf2010.ajward@gmail.com

INTRODUCTION

The increasing demand for sustainable energy has intensified research on low-cost, high-efficiency photovoltaic technologies. Among emerging systems, dye-sensitized and quantum dot-sensitized solar cells (DSSCs and QDSSCs) have attracted considerable attention due to their broad spectral response, tunable optical properties, and simple fabrication processes (Grätzel, M., 2001; Nozik, A. J., 2002). In particular, QDSSCs offer advantages such as high extinction coefficients and size-dependent electronic structures, enabling the possibility of exceeding conventional efficiency limits through mechanisms including multiple exciton generation (MEG) (Klimov, V. I., 2006; Shockley & Queisser, 1961).

The electron transport layer (ETL) plays a critical role in charge separation and collection in these devices. Titanium dioxide (TiO_2) remains the most widely used ETL owing to its wide band gap (~3.2

eV), chemical stability, and favorable electron mobility (O'Regan, B., & Grätzel, M., 1991; Wang, P. etl., 2003). Its mesoporous structure provides a large surface area for quantum dot loading, improving light absorption (Bisquert, J. et al., 2004). However, TiO_2 suffers from limited conductivity and imperfect band alignment with sensitizers, leading to recombination losses and motivating various modification strategies such as doping and surface treatment (Chen & Mao, 2007).

Cadmium-based quantum dots, particularly CdS and CdSe, are widely employed sensitizers because of their strong visible-light absorption and efficient electron injection into TiO_2 (Kamat, P. V., 2008; Hodes, G., 2008). CdS (band gap ≈ 2.4 eV) forms a well-matched heterojunction with TiO_2 and is commonly deposited using chemical bath deposition or the successive ionic layer adsorption and reaction (SILAR) method, allowing controlled growth and interfacial coupling (Lee, H. J. et al., 2009; Santra & Kamat, 2012). Nevertheless, trap-assisted recombination and interfacial defects remain major limitations to device performance.

Sulfur incorporation has been proposed as a strategy to passivate defects, improve band alignment, and enhance carrier transport in CdS systems (Lu, H., et al., 2014). However, the effect of controlled sulfur availability during SILAR growth on recombination dynamics and electron lifetime in TiO_2/CdS QDSSCs remains insufficiently understood. In particular, the relationship between sulfur concentration, charge transport resistance, and flat-band potential has not been systematically investigated.

In this work, CdS quantum dots were grown on TiO_2 photoanodes with controlled sulfur incorporation, and their structural, electronic, and photovoltaic properties were analyzed using electrochemical and spectroscopic techniques. Establishing this relationship provides insight into interfacial charge regulation and offers a practical approach for improving the efficiency and scalability of QDSSCs. The novelty of this study lies in regulating sulfur availability during the SILAR growth of CdS quantum dots and correlating the resulting device performance with recombination resistance, electron lifetime, and flat-band potential. Unlike previous studies that mainly focus on CdS loading, sensitization cycles, or deposition time, this work emphasizes sulfur-mediated interfacial recombination control in TiO_2/CdS QDSSCs.

METHODOLOGY

3.1 Preparation of TiO_2 Plates

TiO_2 paste was prepared by mixing 0.25 g of TiO_2 with 1 ml of 0.1 M HNO_3, one drop of Triton X-100, and one drop of PEG1000, followed by grinding the mixture for 30 minutes using a mortar and pestle. The paste was then applied to pre-cleaned conducting tin oxide (CTO) glass plates (1.0 cm × 2.0 cm) using the doctor blade method. The CTO plates were cleaned in an ultrasonic bath with detergent and distilled water to ensure surface purity. After coating, the TiO_2 films were dried on a hot plate and sintered in a furnace at 450 °C for 45 minutes to achieve the desired properties.

3.2 Preparation of Na_2S and $CdCl_2$ Solutions in Various Concentration

The experiment involved accurately measuring 10.065 g of $CdCl_2$ and 3.902 g of Na_2S using an electronic balance with a precision of ±0.001 g. These compounds were dissolved in 100 mL of distilled water to prepare a 0.5 M solution of Cd^{2+} and S^{2-} ions and the pH of the solution was adjusted to the optimal value of 4.5 by adding 0.01 M NaOH and 0.01 M HCl solutions dropwise, with continuous monitoring to achieve the desired pH (Hodes, G., 2008).

3.3 Preparation of Na_2S solution with S

Sulfur (S) was added in various amounts to a 0.5M Na_2S solution, as specified in the table, and the mixture was stirred for up to 1 hour. This prepared solution was then used in the successive ionic layer adsorption and reaction (SILAR) method to coat CdS on TiO_2 plates.

Table 1: Mass (in grams) of Sulfur in Samples S1 to S7

Sample number	S1	S2	S3	S4	S5	S6	S7
Mass(g)±0.001 g	0.0176	0.0352	0.0705	0.1410	0.2115	0.2820	0

3.4 Deposition of CdS using SLILAR method.

The SILAR technique was utilized to deposit CdS films onto TiO_2 photoanodes. Each immersion in $CdCl_2$ and Na_2S solutions was maintained for one minute. Following each immersion, the photoanodes were rinsed with distilled water to eliminate excess reagents and then air-dried. To achieve uniform film deposition, the photoanodes were alternately immersed in the complementary precursor solution (cationic or anionic), followed by rinsing. This process was repeated ten times to form a multilayer CdS film. Finally, the coated photoanodes were heated at 80°C on a hot plate for 30 minutes to improve the film's adhesion and crystallinity on the substrate.

3.5 Preparation of Electrolyte

In preparation of 2 ml of electrolyte, 0.130 g of Na_2S, 0.128 g of sulfur, and 0.030 g of KCl were dissolved in a solvent mixture comprising 1.4 ml of methanol and 0.6 ml of distilled water. The solution was stirred for 3 hours using a magnetic stirrer to achieve complete dissolution of the salts. Adjustments to the stirring time may be necessary to prevent sulfur precipitation.

3.6 Fabrication of the cell

A counter electrode with a conductive side positioned directly on the CdS-coated TiO_2 film and held in place using clamps. The space between the electrodes was filled with the prepared electrolyte solution, completing the assembly of the Quantum Dot Sensitized Solar Cell.

3.7 Characterization

The fabricated QDSSCs characterized using a VK-PA-100 PV Power Analyzer to obtain J-V curves, enabling the extraction of critical performance metrics such as Photo Conversion Efficiency (PCE), Photo Current Density (Jsc), Photo Voltage (Voc), and Fill Factor (FF). To ensure reproducibility, at least five devices per batch were tested.

Electrochemical Impedance Spectroscopy (EIS) was employed using a frequency response analyzer (Auto-Lab Nova 2.1) to study the charge transport and recombination processes within the CdS QDSSCs. Impedance spectra measured over a frequency range of 0.1 Hz to 1 MHz under constant simulated light intensity at room temperature, providing insights into interfacial charge transfer resistance and recombination dynamics. These findings are vital for optimizing the QDSSC performance.

Incident Photon-to-Current Efficiency (IPCE) measurements will assess the light-harvesting efficiency of the QDSSCs across the solar spectrum. The effectiveness of the quantum dots in capturing sunlight and converting it into photocurrent will be evaluated using a VK-IPCE-10 system.

RESULTS AND DISCUSSION

4.1 Structural and morphological analysis

4.1.1. Morphology of TiO_2 and TiO_2/CdS

Figure 1 shows the scanning electron microscopy (SEM) images of TiO_2, TiO_2/CdS, and sulfur-treated TiO_2/CdS photoanodes at 100,000× magnification. All samples exhibit a porous nanoparticulate morphology typical of doctor-bladed TiO_2 films. After SILAR treatment, slight surface densification and particle aggregation are observed in the TiO_2/CdS and sulfur-treated TiO_2/CdS samples compared with bare TiO_2.

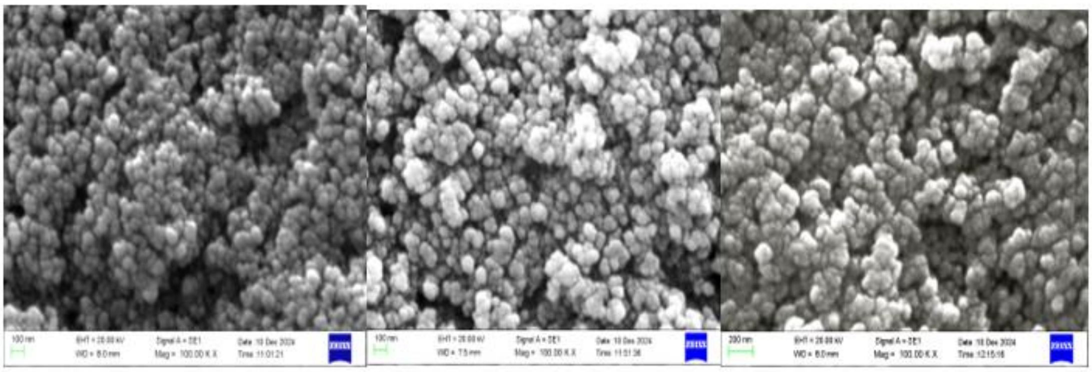

Figure 1: SEM images of TiO_2, TiO_2/CdS and TiO_2/CdS-S

However, these morphological differences are not sufficiently distinct to conclusively confirm CdS deposition or sulfur incorporation from SEM images alone. Therefore, SEM is used here only to compare surface morphology, while direct confirmation of Cd and S distribution would require elemental analysis such as SEM–EDS (Li, W., et al., 2018).

4.1.2 XRD

The XRD patterns are dominated by diffraction peaks corresponding to anatase TiO_2. The main TiO_2 peaks observed at 25.3°, 37.8°, 48.0°, 53.9°, 55.1°, 62.7°, and 75.1° can be assigned to the (101), (004), (200), (105), (211), (204), and (215) planes of anatase TiO_2 (JCPDS No. 21-1272). In the TiO_2/CdS and sulfur-treated TiO_2/CdS samples, distinct CdS-related peaks are weak or not clearly separated from the dominant TiO_2 background. This may be due to low CdS loading, nanoscale crystallite size, overlap between TiO_2 and CdS reflections, or the partially amorphous nature of SILAR-deposited CdS. Therefore, the XRD results are interpreted as supporting structural information rather than conclusive confirmation of crystalline CdS formation or sulfur incorporation.

The weak or unresolved CdS-related features also limit reliable crystallite size estimation for CdS using the Scherrer equation. Therefore, crystallite size calculation was not performed for the CdS phase in the thin-film samples. More accurate crystallite size and phase analysis would require powder samples or thicker films followed by proper annealing under an inert atmosphere (Li, W., et al., 2018).

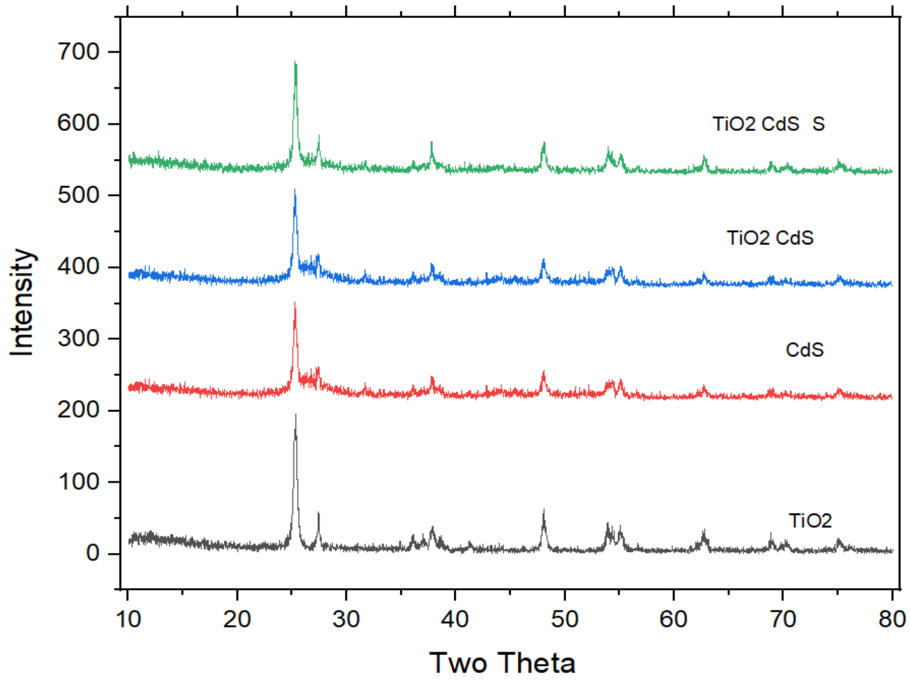

Figure 2: X-ray diffraction (XRD) patterns of TiO_2, CdS, TiO_2/CdS, and TiO_2/CdS with added sulfur (S).

4.1.3 FTIR

FTIR spectroscopy was used to examine surface functional groups and possible chemical changes after CdS deposition and sulfur treatment. Figure 3 presents the FTIR spectra of TiO_2, TiO_2/CdS, and sulfur-treated TiO_2/CdS photoanodes.

The FTIR spectra of TiO_2, TiO_2/CdS, and sulfur-treated TiO_2/CdS show broad absorption bands around 3400 cm^{-1} and 1600 cm^{-1}, which are attributed to O–H stretching and bending vibrations of adsorbed water or surface hydroxyl groups. The strong intensity of these bands indicates that residual moisture may still be present in the samples. Therefore, the FTIR results should be interpreted with caution. Although weak variations are observed in the lower wavenumber region, these changes are not sufficient to conclusively prove CdS formation or sulfur incorporation. Further FTIR measurements after complete drying of the samples are required for more reliable functional group analysis. Thus, the FTIR results are treated as supporting evidence for possible surface modification, while the influence of sulfur treatment is mainly evaluated using the photovoltaic, EIS, and Mott–Schottky results.

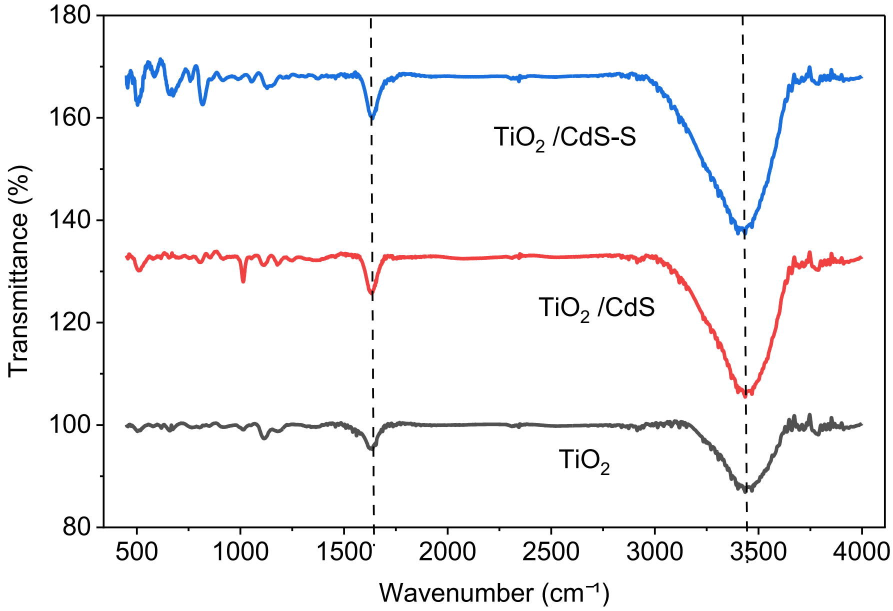

Figure 3: FTIR spectra of TiO_2, TiO_2/CdS, and sulfur-added TiO_2/CdS.

The SEM, XRD, and FTIR results show only subtle changes among TiO_2, TiO_2/CdS, and sulfur-treated TiO_2/CdS samples. This may be due to low CdS loading, nanoscale or partially amorphous CdS formation, and the dominance of the TiO_2 matrix in the structural spectra. Therefore, these techniques are considered supportive rather than conclusive evidence for CdS and sulfur incorporation. The influence of sulfur treatment is mainly supported by the consistent improvement in photovoltaic performance, recombination resistance, electron lifetime, and flat-band potential. Future studies using SEM–EDS, Raman spectroscopy, and XRD of powder or thicker annealed films would further confirm the elemental composition and phase structure.

4.2 Band alignment analysis (Mott-Schottky)

The Mott–Schottky (MS) analysis provides valuable insight into the electrochemical properties of the TiO_2-based photoanodes by enabling determination of the flat-band potential (Vfb) and charge carrier density (Nd), which directly influence charge transfer efficiency in quantum dot-sensitized solar cells (QDSCs). The flat-band potential represents the potential at which no space-charge region exists within the semiconductor and serves as an indicator of the conduction band edge position, thereby governing electron injection and transport. It is determined from the linear region of the MS plots using the relation,

$$\frac{1}{C^2} = \frac{2}{e\epsilon\epsilon_0 N_d}(V - V_{fb})$$

Here, Vfb is obtained by extrapolating the linear region of the $1/C^2$ vs. potential plot to the x-axis. A positive shift in Vfb indicates favorable band-edge realignment and improved interfacial energetics (Wang, X., et al., 2018).

From the x-intercepts of the plots, the Vfb values were found to be −0.747 V for TiO_2, −0.691 V for TiO_2/CdS, and −0.588 V for sulfur-treated TiO_2/CdS (vs Ag/AgCl). The progressive positive shift in Vfb upon CdS sensitization and sulfur treatment indicates favorable modification of interfacial band alignment, consistent with literature reports on surface passivation and dipole-induced band-edge realignment. The carrier density (Nd), calculated from the slope of the MS plots using

$$N_d = \frac{2}{e\epsilon\epsilon_0}\left(\frac{d\left(1/C^2\right)}{dV}\right)^{-1}$$

where e=1.6×10−19e C is the elementary charge, ϵ is the relative permittivity (≈80 for TiO_2 and ≈5.7for CdS), and ϵ0=8.85×10−14F/cm is the permittivity of free space. The term d(1/C2)/dV represents the slope of the Mott-Schottky plot.[16] CdS sensitization leads to an increase in the apparent carrier density, while the reduction in apparent carrier density after sulfur treatment does not indicate poorer conductivity. Instead, it reflects suppression of trap-state charge accumulation at the TiO_2/CdS interface. Sulfur incorporation passivates surface defects that normally store electrons, thereby decreasing the measured capacitance-derived carrier density while simultaneously reducing recombination. Consequently, charge transport becomes more efficient despite the lower apparent Nd (Wang, X., et al., 2018).

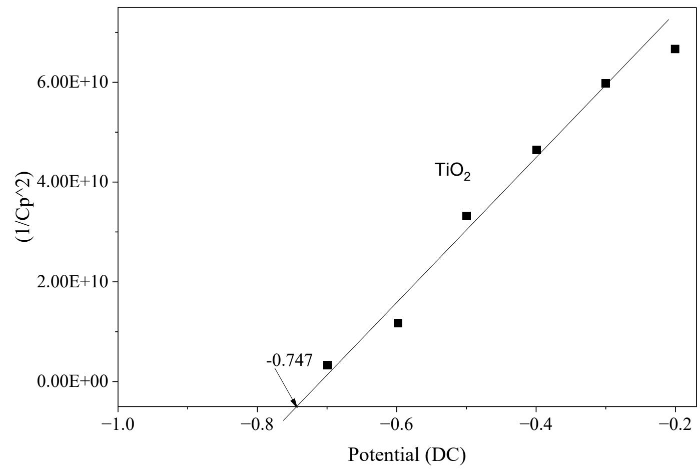

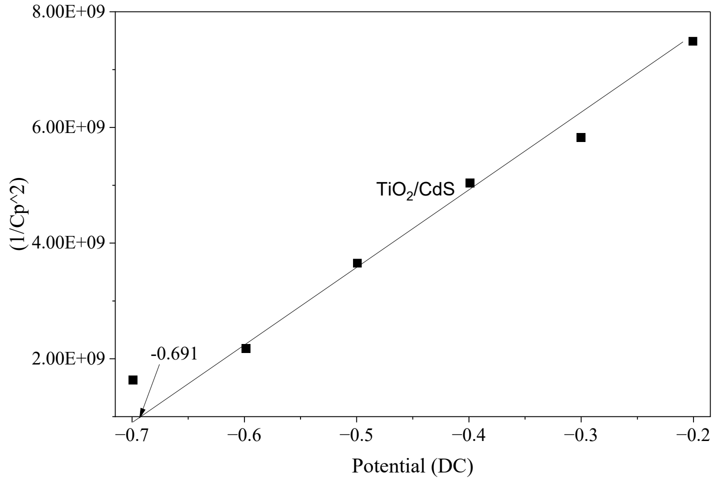

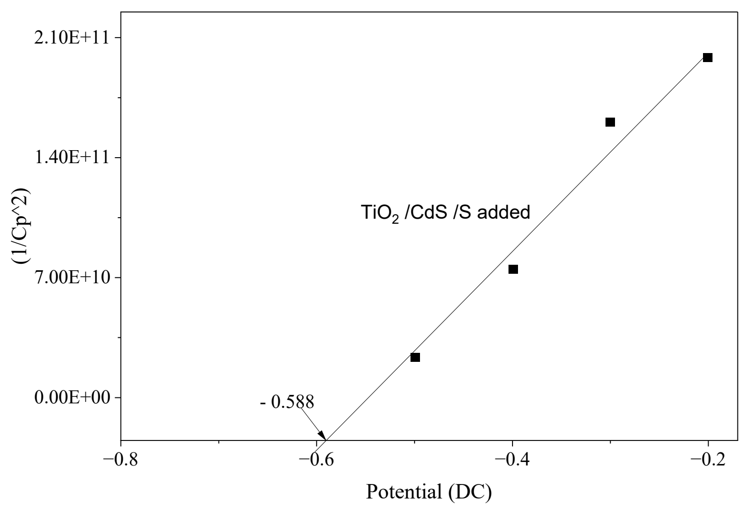

Figure 4: Mott-Schottky ($1/C^2$ vs. Potential) Plots of Bare TiO_2, CdS-Sensitized TiO_2 (TiO_2/CdS), and Sulfur-Doped CdS-Sensitized TiO_2 (TiO_2/CdS-S) Electrodes

Table 2: Flat Band Potentials, Carrier density of TiO_2, TiO_2/CdS, and TiO_2/CdS-S

Sample	Flat band potential (Vfb) (V vs. Ag/AgCl)	Slope ($d(1/C^2)/dV$) $\times 10^{11}$ ($F^{-2} \wedge V^{-1}$)	Carrier density (N_d) cm^{-3}
TiO_2	-0.747	1.28×10^{11}	1.38×10^{19}
TiO_2 / CdS	-0.691	1.53×10^{10}	1.15×10^{20}
TiO_2/ CdS S	-0.588	5.15×10^{11}	3.42×10^{18}

As shown in Figure 4, the corresponding values summarized in Table 2 were obtained in this research study. Table 2 presents the Mott–Schottky parameters of TiO_2, TiO_2/CdS, and sulfur-treated TiO_2/CdS photoanodes. The flat-band potential shifts positively from −0.747 V for TiO_2 to −0.691 V after CdS sensitization and further to −0.588 V upon sulfur treatment (vs Ag/AgCl), indicating progressive modification of interfacial band alignment. The TiO_2/CdS electrode exhibits the lowest slope (1.53×10^{10} F^{-2} V^{-1}) and the highest apparent carrier density (1.15×10^{20} cm^{-3}), reflecting enhanced electron availability due to CdS sensitization. In contrast, sulfur-treated TiO_2/CdS shows a higher slope (5.15×10^{11} F^{-2} V^{-1}) and reduced carrier density (3.42×10^{18} cm^{-3}), suggesting suppression of trap-assisted charge accumulation and improved interfacial order.

4.3 Charge recombination dynamics (Electrochemical impedance spectroscopy)

Electrochemical impedance spectroscopy (EIS) was employed to evaluate interfacial charge-transfer characteristics and recombination kinetics of the S-doped CdS QD-sensitized photoanodes (S1–S7). The fitted series resistance (Rs) reflects the ohmic contributions from the FTO substrate, contacts, and electrolyte, where a clear minimum is observed for S4 (33.4 Ω) compared to S1 (115 Ω) and S7 (94 Ω), indicating improved electrical pathways and reduced transport losses at the optimized sulphur condition.

The improvement in photovoltaic performance originates from suppression of interfacial trap-assisted recombination. The improvement in EIS and photovoltaic performance suggests that sulfur treatment may reduce interfacial recombination and improve charge transport. However, since direct elemental confirmation was not obtained in this study, this mechanism should be interpreted as a probable explanation based on electrochemical behavior rather than direct structural proof. The charge-transfer/recombination resistance (Rp) increases markedly with sulphur incorporation and reaches the highest value for S4 (216.4 kΩ), followed by S5 (206.6 kΩ) and S3 (188.6 kΩ), while the lowest Rp is obtained for the undoped/least-protected condition S7 (76.2 kΩ). The elevated Rp for S4 suggests strong suppression of interfacial electron back-transfer to the electrolyte, consistent with improved surface passivation and favorable band alignment at the TiO_2/CdS/electrolyte interface.

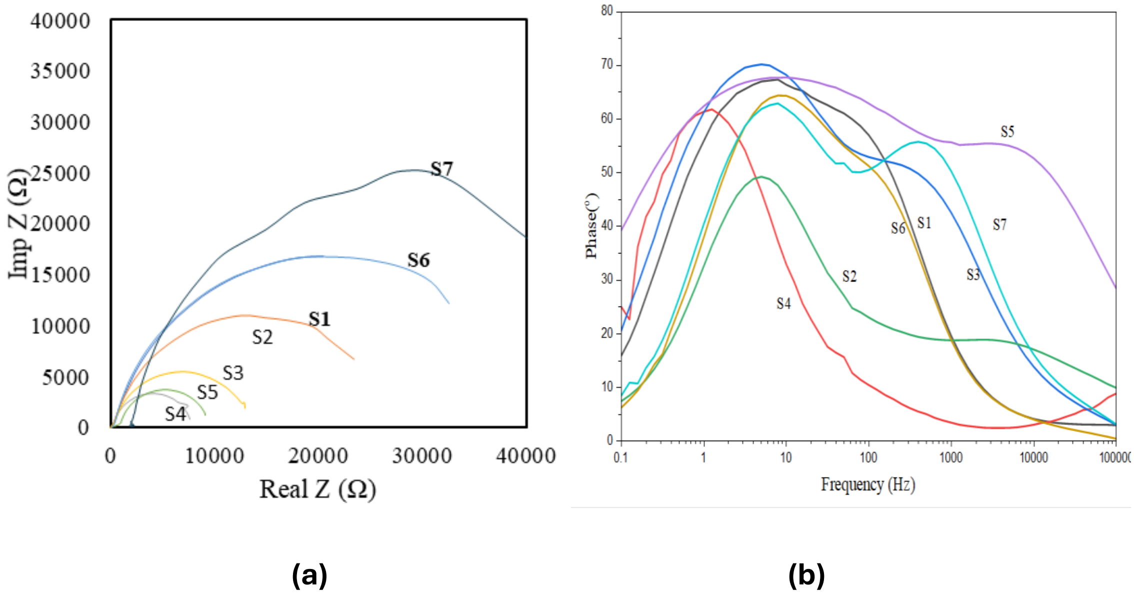

Figure 5: (a) Impedance spectra characteristics of TiO_2/CdS with varying sulfur (S) mass in Na_2S. (b) Wavelength and Phase of TiO_2/CdS with varying sulfur (S) mass in Na_2S.

Table 3. Parameters of equivalent circuit for different QDSC configuration

	S1	S2	S3	S4	S5	S6	S7
Rs(Ω)	115	62	71.3	33.4	47.4	39	94
Rp(kΩ)	108	166.9	188.57	216.4	206.6	156.1	76.2
CPE	0.524	0.866	0.811	0.713	0.745	0.866	0.898
Peak frequency (Hz)	6.309	5.011	3.981	1.000	1.584	7.943	9.143
Phase (°)	67.216	61.254	69.962	49.293	67.686	64.401	62.942
Electron lifetime	0.0252	0.0317	0.0399	0.1591	0.1004	0.0200	0.0174

Figure 6 illustrates the schematic circuit diagram of the equivalent circuit for a quantum dot-sensitized solar cell. In this model, Rs represents the series resistance, Rp denotes the parallel (shunt) resistance, and CPE corresponds to the constant phase element.

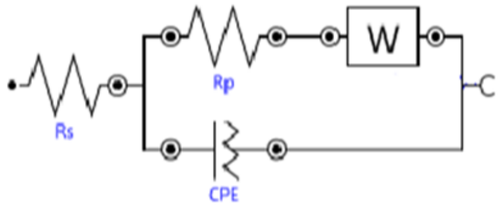

Figure 6: Equivalent circuit

The characteristic recombination frequency derived from Bode analysis further supports this trend. The peak frequency decreases to 1.0 Hz for S4, corresponding to the longest electron lifetime τ=1/(2πfpeak) of 0.1591 s, whereas higher peak frequencies such as 9.143 Hz (S7) and 7.943 Hz (S6) yield much shorter lifetimes (0.0174 s and 0.0200 s, respectively), indicating accelerated recombination. The constant phase element (CPE) values (0.524–0.898) confirm non-ideal capacitive behavior typical of porous semiconductor electrodes, where deviations from ideality arise from surface roughness, distributed trap states, and interfacial heterogeneity; notably, the lower CPE for S1 (0.524) implies a more heterogeneous interface compared with the more ideal behavior observed for S6–S7 (~0.87–0.90). Overall, the simultaneous reduction in Rs, increase in Rp, and prolonged electron lifetime for S4 demonstrate that the optimized sulphur incorporation effectively enhances charge transport while suppressing recombination, providing an electrochemical basis for the improved photovoltaic output of the corresponding devices.

4.4 Photovoltaic performance (I–V Characteristics of CdS QDSSCs)

Figure 7 and Table 4 illustrate the photovoltaic performance of QDSSCs prepared with different sulfur contents. Significant improvements are observed in sample S4, where voltage increases from 436.7 mV to 470.8 mV (7.8% increase), current density rises from 2.265 mA to 4.176 mA (84.5% increase), and efficiency doubles from 0.262% to 0.519% (98.5% increase), compared to S7 (0 g). These enhancements are attributed to incorporation of sulfur in CdS QDs improving light absorption and facilitating charge transport. However, beyond the optimal sulfur concentration of 0.1410g (e.g., S5 and S6), the performance plateaus or slightly decreases, likely due to excessive sulfur causing aggregation or hindering charge transfer. The lowest current output is observed at 0 g (S7), highlighting the critical role of sulfur in enhancing QDSSC functionality.

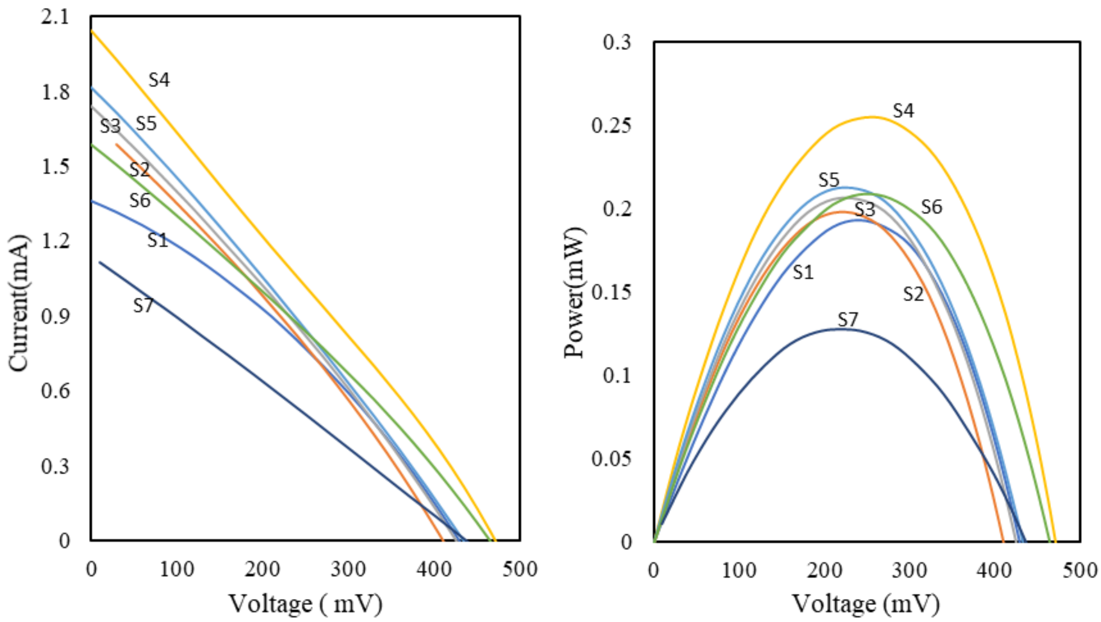

(a) (b)

Figure 7: (a) Current–voltage characteristics of TiO_2/CdS QDSSCs prepared with varying sulfur content (mass listed in Table 1), under simulated AM 1.5G illumination (100 mW cm^{-2}).

(b) Voltage–power characteristics for the same samples

It illustrates that sulfur enhances QDSSC efficiency by improving light absorption, charge transfer, and surface passivation. However, an optimal sulfur concentration (0.1410g) supposed to maximizes efficiency by reducing defects and recombination. At higher concentrations, defects and structural issues may arise, leading to electron trapping leading to lower efficiency. Overall, the results highlight the importance of sulfur-content optimization, with S4 showing the best photovoltaic performance among the investigated samples.

The power-voltage (P-V) graph compares the performance of QDSSCs with varying sulfur (S) concentrations, highlighting the relationship between power output and voltage. Among the samples, the highest power output is achieved at 0.1410g of sulfur (S4), while the lowest is observed at 0 g of sulfur (S7). The peak power for S4 is significantly higher than S7(98.44%), demonstrating the critical role of sulfur in enhancing the solar cell's performance through improved light absorption, charge transfer, and reduced recombination. In contrast, the S7 sample lacks these advantages, resulting in minimal power generation.

Table 4: Photovoltaic Parameters of CdS Quantum Dot-Sensitized Solar Cells

Sample Number	S1	S2	S3	S4	S5	S6	S7
Voltage(mV)	428.6	409.9	424.7	470.8	432.9	464.4	436.7
Current Density (mA m^{-2})	2.781	3.434	3.552	4.176	3.701	3.235	2.265
Fill Factor	33.0	28.7	27.9	26.4	27.0	28.3	26.5
Efficiency (%)	0.394	0.404	0.421	0.519	0.433	0.426	0.262
Maximum Power	0.193	0.198	0.206	0.254	0.212	0.209	0.128

The use of power-voltage plots is essential in QDSSCs as they provide a clear understanding of the cell's efficiency and operating conditions. While current-voltage plots indicate the potential and current capabilities, P-V plots reveal the maximum power point (MPP) the voltage and current at which the solar cell operates most efficiently. This information is crucial for optimizing the design and tuning the parameters to maximize energy output, making the P-V graph a critical tool in evaluating and improving QDSSC performance.
Although the absolute efficiency obtained in this study is lower than highly optimized CdS-based QDSSCs reported in the literature, the present work focuses on the relative improvement caused by controlled sulfur treatment under the same fabrication conditions. The efficiency increased from 0.262% for the untreated/zero-sulfur sample to 0.519% for the optimized S4 sample, corresponding to an approximately 98.5% relative enhancement. Therefore, the significance of the result lies not in achieving record efficiency, but in demonstrating that sulfur availability during SILAR deposition strongly influences recombination dynamics and device output.

4.5 Spectral response (Incident Photon-to-Current Efficiency of QDSSCS)

The Incident Photon-to-Current Efficiency (IPCE) spectra in Figure 8 provide a detailed evaluation of the wavelength-dependent photocurrent generation in TiO_2/CdS Quantum Dot-Sensitized Solar Cells (QDSSCs) with varying sulfur (S) concentrations in CdS QDs. All samples show a decrease in IPCE with increasing wavelength, consistent with the absorption characteristics of CdS quantum dots, which have a bandgap energy of approximately 2.4 eV. This decline reflects the limited absorption and exciton generation at longer wavelengths, highlighting the need for precise quantum dot size control to extend spectral response.

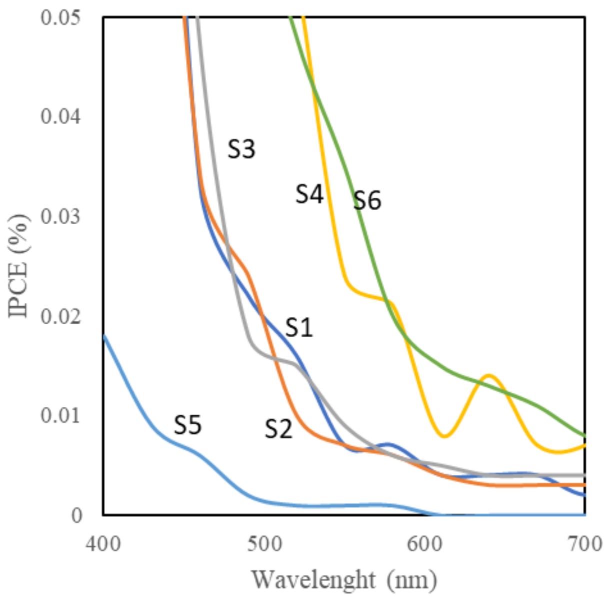

Figure 8: Wavelength vs Photocurrent Efficiency (IPCE) for TiO_2/CdS QDSSCs with the variation of sulfur

Among the different sulfur concentrations, S4 and S6 exhibit pronounced peaks within the 610–670 nm range, suggesting enhanced light-harvesting and efficient charge separation. This can be attributed to an optimal size distribution of CdS quantum dots, promoting efficient photon absorption and electron injection into the TiO_2 conduction band.

The peak in S4, in particular, indicates favorable size quantization effects that align well with the incident light spectrum, maximizing photocurrent generation. This suggests a reduced recombination rate due to improved interfacial energy states and optimized charge transport pathways.
In contrast, S1 and S5 show the lowest IPCE values across all wavelengths, indicating poor light absorption and inefficient charge separation. The absence of significant peaks suggests suboptimal quantum dot growth, possibly due to agglomeration or non-uniform size distribution, leading to increased recombination losses. S2 and S3 display moderate IPCE values with relatively flat spectral profiles, reflecting less effective size quantization and reduced quantum confinement effects. The IPCE measurement in the present study was limited to the 400–700 nm visible region. Extension of the measurement range up to approximately 1100 nm would provide additional information on low-energy photon response and possible defect-related contributions.
These findings underscore the crucial role of sulfur concentration in tuning the optical and electronic properties of CdS quantum dots. The superior performance of S4 demonstrates that precise sulfur content control enhances quantum dot size distribution, leading to improved light absorption and charge carrier dynamics. This emphasizes the importance of strategic quantum dot engineering for optimizing the photovoltaic performance of TiO_2/CdS QDSSCs.

CONCLUSION

Controlled sulfur addition during the SILAR deposition process influenced the photovoltaic and electrochemical performance of TiO_2/CdS quantum dot-sensitized solar cells. The optimized sample showed an efficiency improvement from 0.262% to 0.519%, together with increased photocurrent, higher open-circuit voltage, greater recombination resistance, and longer electron lifetime. These results suggest that sulfur treatment may suppress interfacial recombination and improve charge transport within the TiO_2/CdS photoanode system.
However, SEM, XRD, and FTIR analyses did not provide conclusive evidence for CdS crystallinity or sulfur incorporation because the structural and spectroscopic differences among the samples were relatively small. The CdS phase may be amorphous or poorly crystalline, possibly due to insufficient annealing temperature. Therefore, further characterization using SEM–EDS, Raman spectroscopy, and XRD analysis of powder or thicker annealed films is required to confirm elemental composition and phase formation.
Overall, the electrochemical and photovoltaic results indicate that controlled sulfur treatment is a promising approach for improving TiO_2/CdS QDSSC performance, although further structural confirmation is necessary to fully validate the proposed mechanism.

REFERENCES

[1] Grätzel, M. (2001). Dye-sensitized solar cells. *Journal of Photochemistry and Photobiology C: Photochemistry Reviews, 4*(2), 145-153.
[2] Nozik, A. J. (2002). Quantum dot solar cells. *Physica E: Low-dimensional Systems and Nanostructures, 14*(1-2), 115-120.
[3] Klimov, V. I. (2006). Detailed-balance power conversion limits of nanocrystal quantum dot solar cells. *Applied Physics Letters, 89*(12), 123118.
[4] Shockley, W., & Queisser, H. J. (1961). Detailed balance limit of efficiency of p-n junction solar cells. *Journal of Applied Physics, 32*(3), 510-519.

[5] O'Regan, B., & Grätzel, M. (1991). A low-cost, high-efficiency solar cell based on dye-sensitized colloidal TiO_2 films. *Nature, 353*(6346), 737-740.

[6] Wang, P., Zakeeruddin, S. M., Moser, J. E., Humphry-Baker, R., & Grätzel, M. (2003). A stable quasi-solid-state dye-sensitized solar cell with an amphiphilic ruthenium sensitizer and polymer gel electrolyte. *Nature Materials, 2*(6), 402-407.

[7] Bisquert, J., Cahen, D., Hodes, G., Rühle, S., & Zaban, A. (2004). Physical chemical principles of photovoltaic conversion with nanoparticulate, mesoporous dye-sensitized solar cells. *Journal of Physical Chemistry B, 108*(24), 8106-8118.

[8] Chen, X., & Mao, S. S. (2007). Titanium dioxide nanomaterials: Synthesis, properties, modifications, and applications. *Chemical Reviews, 107*(7), 2891-2959.

[9] Kamat, P. V. (2008). Quantum dot solar cells: Semiconductor nanocrystals as light harvesters. *Journal of Physical Chemistry C, 112*(48), 18737-18753.

[10] Hodes, G. (2008). Comparison of dye- and semiconductor-sensitized porous nanocrystalline liquid junction solar cells. *Journal of Physical Chemistry C, 112*(46), 17778-17787.

[11] Lee, H. J., Yum, J. H., Moon, S. J., et al. (2009). CdS quantum dot-sensitized solar cells exceeding 4% efficiency employing an organic hole conductor. *Journal of Physical Chemistry C, 113*(46), 19921-19927.

[12] Santra, P. K., & Kamat, P. V. (2012). Mn-doped quantum dot sensitized solar cells: A strategy to boost efficiency over 5%. *Journal of the American Chemical Society, 134*(50), 2508-2514.

[13] Lu, H., Tian, J., Cao, G., et al. (2014). Sulfur-doped TiO_2 nanoparticles for photoelectrochemical water splitting. *Journal of Physical Chemistry C, 118*(47), 25329-25337.

[14] Li, W., Ding, H., Ji, H., Dai, W., Guo, J., & Du, G. (2018). Photocatalytic degradation of tetracycline hydrochloride via a CdS-TiO2 heterostructure composite under visible light irradiation. Nanomaterials, 8(6), 415.

[15] Wang, X. et al. (2018) – "Enhanced Photoelectrochemical Performance of CdS Quantum Dot-Sensitized TiO_2." *Journal of Solar Energy Materials*.

[16] Zhang, Y. et al. (2017) – "Charge Transfer in CdS-Sensitized TiO_2 Nanostructures." *ACS Applied Materials & Interfaces*.

[17] Kunnamareddy, M., Rajendran, R., Sivagnanam, M., Rajendran, R., & Diravidamani, B. (2021). Nickel and sulfur codoped TiO 2 nanoparticles for efficient visible light photocatalytic activity. *Journal of Inorganic and Organometallic Polymers and Materials*, *31*, 2615-2626.

[18] O'Hayre, R., Nanu, M., Schoonman, J., & Goossens, A. (2007). Mott− Schottky and charge-transport analysis of nanoporous titanium dioxide films in air. The Journal of Physical Chemistry C, 111(12), 4809-4814.

[19] Zhu, Q., Wang, J., Chen, S., Fu, H., Zhang, J., Gao, H., & Liao, Y. (2022). Effect of the organic sulfur source on the photocatalytic activity of CdS. *RSC advances*, *12*(18), 11262-11271.

[20] Chen, Y., Qin, Z., Chen, T., Su, J., Feng, X., & Liu, M. (2016). Optimization of $(Cu_2Sn)_xZn_{3(1-x)}S_3$/CdS pn junction photoelectrodes for solar water reduction.

SOLVING DETERMINISTIC MULTI-OBJECTIVE ASSIGNMENT PROBLEMS USING ANT COLONY OPTIMIZATION ALGORITHM

C. P. S. Pathirana[1*] and W. B. Daundasekera[2]

[1]Department of Mathematics & Philosophy of Engineering, Faculty of Engineering Technology, The Open University of Sri Lanka, Nawala, Nugegoda, Sri Lanka
[2] Department of Mathematics, Faculty of Science, University of Peradeniya, Peradeniya, Sri Lanka

ABSTRACT

This study is proposing a metaheuristic algorithm known as Ant Colony Optimization Algorithm (ACOA) to solve deterministic Multi-Objective Assignment Problems (MOAPs). While single-objective assignment problems have only one objective to optimize, MOAPs have several conflicting objectives to optimize simultaneously, such as minimizing production time and maximizing the productivity. ACOA is well-suited to solve this type of problems to a certain degree of accuracy because of the adaptive search and the collaborative learning. In this study, the ACOA is applied to seek a feasible near optimal solution to the deterministic assignment model, where in the implementation of the algorithm, the artificial ants construct assignments based on pheromone trails and heuristic desirability derived from the probabilistic estimates. The mechanism of pheromone evaporation and probabilistic path selection permit the algorithm to locate the near optimal solution while adhering to a set of constraints. The proposed algorithm is coded in Python programming language and the efficiency of the algorithm in solving MOAPs is compared with an existing prominent method known as Technique for an Order of Preference by Similarity to Ideal Solution (TOPSIS). The proposed Multi-Objective Ant Colony Optimization Algorithm (MOACOA) is proven to be capable of solving large scale MOAPs in less computational time compared to the TOPSIS method. The extension of this study can focus on solving stochastic MOAPs.

Keywords: Ant colony Optimization, Assignment problem, Cost matrix, Multi-objective, Pheromone evaporation.

----

*cppat@ou.ac.lk

INTRODUCTION

Decision-making in real-world environments often involves allocating a set of limited resources to a set of tasks while simultaneously optimizing multiple objectives which are conflicting in nature. Production planning, personnel assignment, transportation, machine allocation, and project management are just a few of the many areas where this occurs. The classical Assignment Problem (AP) is a well-known optimization problem that determines the optimal one-to-one assignment of a set of agents (e.g., workers, machines, etc.) to an equal number of tasks, with the objective of minimizing total assignment cost or maximizing total profit, subject to the constraints that each agent is assigned to exactly one task and each task is performed by exactly one agent. However, in practical situations, decision-makers are rarely concerned with a single criterion. Multiple performance measures such as cost, time, efficiency, reliability, and risk must often be considered concurrently. In Multi-Objective Assignment Problem (MOAP), the goal is to determine the optimal assignment that achieves a balance among several conflicting objectives (Alaya et al, 2007). The computational time of solving MOAP increases with the problem size and the number of objectives, and traditional algorithms are computationally demanding to solve large scale problems. To address this challenge, metaheuristic algorithms have been employed due to their ability to obtain high-quality near-optimal solutions within reasonable computational time. In this study, a metaheuristic algorithm, named Ant Colony Optimization Algorithm (ACOA), was considered to obtain the optimal solution to the MOAP. Further, the study shows that the proposed algorithm is computationally efficient in solving the MOAP. The proposed approach seeks to identify near-optimal compromise solutions among a large number of feasible assignments, recognizing that exact optimality is often computationally impractical for large-scale MOAPs.

The ACOA was first proposed by Dorigo et al. to solve NP-hard optimization problems such as the Traveling Salesman Problem, and it has since been extended to address a wide range of discrete optimization problems [(Dorigo et al., 1991), (Dorigo et al., 1999), (Rekaya et al., 2013) and (Monteriro et al., 2012)]. Ant Colony Optimization (ACO) is a metaheuristic introduced by Marco Dorigo, inspired by the collective foraging behavior of biological ants (Dorigo et al., 1991). The algorithm was originally developed in 1992 as part of Dorigo’s PhD research [(Dorigo et al., 1991) and (Dorigo, 1992)]. ACO is based on the natural process by which ants search for shortest paths between their colony and food sources. The field of ant colony optimization, which is a biologically inspired method, has been shaped by a number of researchers who have made valuable contributions to the development and success of the field. The field of ‘‘ant colony algorithms’’ studies models derived from the observation of real ants’ behavior and uses these models as a source of inspiration for the design of novel algorithms to solve optimization and distributed control problems [(Dorigo et al., 1991), (Dorigo, 1992) and (Alizaden et al, 2014)]. The ACOA is a probabilistic technique which can be used to find the optimal solution of the AP. Recent studies [(Blum, 2005), (Gulben, 2015) and (Rekaya, 2013)] have demonstrated that the Ant Colony Optimization Algorithm (ACOA) performs competitively compared to exact methods and other metaheuristic approaches when solving large-scale assignment problems. Although exact methods guarantee optimal solutions, they often become computationally impractical for high-dimensional problems. In contrast, ACOA is capable of producing high-quality near-optimal solutions within a significantly less computational time, making it a practical and efficient approach for real-world task scheduling problems subject to operational constraints.

The first extensions of ACOA for Multi-Objective Ant Colony Optimization Algorithm (MOACOA) were proposed at the end of the 1990s. Its initial application area was single objective AP. However, the existing ACOA was extended to solve MOAP, where the quality of candidate solutions is evaluated according to several conflicting objectives. One of the fundamental challenges in Multi-Objective Ant Colony Optimization (MOACO) is the representation and management of pheromone information for multiple objectives. Two main strategies have been proposed to overcome the challenge: use of a single pheromone matrix and use of multiple pheromone matrices (Maniezzo et al., 2010). When a single pheromone matrix is employed, pheromone updates are typically performed using some or all non-dominated solutions obtained during the search (Iredi et al., 2001). In contrast, approaches based on multiple pheromone matrices, generally assign a separate pheromone structure to each objective, with pheromone updates guided by elite solutions corresponding to the individual objectives (Alaya et al., 2007; Doerner et al., 2004). During the solution construction process, information from multiple pheromone and heuristic matrices is usually combined through weighting schemes to balance the influence of the different objectives (Maniezzo et al., 2010). Although the behavior of a single ant is relatively simple, the cooperative interaction among many ants gives rise to an intelligent and adaptive search mechanism capable of solving complex optimization problems (Syariza et al., 2018). This self-organizing behavior has motivated the development of ACO-based algorithms for a wide range of combinatorial and multi-objective optimization problems, including assignment, scheduling, routing, and resource allocation.

An ant colony is highly organized, in which one ant interacts with others through pheromone in perfect harmony. While perhaps seemingly simple, this is indeed a very complex behavior (White, 1984). The complex behavior of ants has inspired researchers to find solutions to certain optimization problems. The ACOA is developed based on biological behavior of ants seeking a path between their colony and source food (Pathirana et al., 2024). In this study, Multi-Objective Ant Colony Optimization Algorithm (MOACOA) is proposed which is a probabilistic approach for finding the optimal solution of the MOAP. The optimal assignment found by applying this proposed method is verified by applying an existing method known as Technique for an Order of Preference by Similarity to Ideal Solution (TOPSIS) (Hwang et al. 1981; Starkweather, 1991).

The TOPSIS method was first proposed by Hwang and Yoon as a distance-based Multi-Criteria Decision-Making (MCDM) approach. TOPSIS is particularly useful in problems where alternatives must be ranked or selected based on multiple criteria, such as assignment problems, resource allocation, and decision optimization (Hwang et al. 1981). The fundamental principle of TOPSIS is that the chosen alternative should have the shortest distance from the positive ideal solution (PIS) and the farthest distance from the negative ideal solution (NIS). The PIS represents the best possible performance across all criteria, while the NIS represents the worst. Since its introduction, TOPSIS has become one of the most widely used methods. In multi-objective assignment problems (MOAP), TOPSIS is often used as a decision-support tool to select the most preferred assignment from a set of Pareto-optimal or feasible solutions generated by optimization algorithms (Behzadian et al., 2012). These strengths make TOPSIS particularly suitable for evaluating solutions obtained from algorithms such as genetic algorithms, ant colony optimization, and other metaheuristic approaches. In the context of the present research, TOPSIS is employed as a multi-criteria decision-making framework to evaluate and select optimal or near-optimal assignment solutions. TOPSIS uses as a suitable decision-support technique for solving multi-objective assignment problems. In this research, computational results demonstrate that the proposed algorithm is capable of solving large-scale MOAPs with significantly less computational time than the TOPSIS method.

MATERIALS AND METHODS

The general formulation of the mathematical model of the MOAP can be represented as below.
Parameters:

m	number of objectives
n	number of agents/number of tasks
c_{ij}^k	cost of assigning j^{th} task to i^{th} agent for k^{th} objective

$$\text{Min } Z^k(x) = \sum_{i=1}^{n}\sum_{j=1}^{n} c_{ij}^k x_{ij} \quad ; \quad k = 1, 2, \dots, m$$

subject to the constraints

$$\sum_{j=1}^{n} x_{ij} = 1 \qquad ; i = 1, 2, \dots, n \quad \text{- Agent assigned to a task}$$

$$\sum_{i=1}^{n} x_{ij} = 1 \qquad ; j = 1, 2, \dots, n \quad \text{- Task assigned to an agent,}$$

where x_{ij} is defined as

$$x_{ij} = \begin{cases} 1, & \text{if } i^{th} \text{agentis assigned to } j^{th} \text{task,} \\ 0, & \text{if } i^{th} \text{ agent is not assigned to } j^{th} \text{ task.} \end{cases}$$

Furthermore, the standard matrix of the multi-objective assignment problem is as follows:

$$[c_{ij}^k]_{n\times n} = \begin{pmatrix} c_{11}^k & c_{12}^k & \cdots & c_{1n}^k \\ c_{21}^k & c_{22}^k & \cdots & c_{2n}^k \\ \vdots & \vdots & \ddots & \vdots \\ c_{n1}^k & c_{n2}^k & \cdots & c_{nn}^k \end{pmatrix}_{n\times n} \quad ; k = 1, 2, \dots, m.$$

In this model all parameters are assumed to be deterministic.

Considering the proposed method of constructing the probabilistic solution for the ant colony system, when using multiple matrices, where each matrix is corresponding to a specific objective, the matrices are added together using weighted sum, where weights are assigned according to the priorities given to the objectives. In this study, a linear aggregation approach is adopted, as the proposed ACOA ensures that all pheromone values are maintained within the same range. Within the ACOA framework, the probabilistic solution construction mechanism involves assigning an initial pheromone value and estimating the selection probability for each candidate solution. In the proposed method, the procedure begins with the first row of each Assignment Cost Matrix (ACM).

Initially, transition probabilities (p_{ij}^q) of all paths in the first row of the linear aggregation of ACMs are calculated. Based on these probabilities, the cumulative probabilities (CP) for that row will also be calculated. For the random selection of the new path, a random number between 0 and 1 is generated uniformly for each selected path. Comparing the CP and the generated random number the new path is determined. If the comparison between the CP and the generated random number across all candidate paths does not yield a unique path, that is, if multiple paths become candidates, the pheromone levels are updated and the transition probabilities are recomputed accordingly, and then the process described earlier will be repeated. This procedure is repeated for the corresponding row of the linearly aggregated ACMs until the comparison converges to a unique shortest path. After selecting the shortest path for the corresponding row, this process is repeated sequentially for the remaining rows of the ACMs as well.

The transition probability of the q^{th} ant moving from agent i to task j is as follows (Gulben, 2015; Manuel et al. 2010)]:

$$p_{ij}^q = \frac{(\sum_{l=1}^{k} w_l \tau_{ij}^l)^\alpha (\sum_{l=1}^{k} w_l \eta_{ij}^l)^\beta}{\sum_{j\in N_i^q}[(\sum_{l=1}^{k} w_l \tau_{ij}^l)^\alpha (\sum_{l=1}^{k} w_l \eta_{ij}^l)^\beta]},$$

where N_i^q is the feasible neighborhood of ant q and $\eta_{ij} = 1/c_{ij}$, where c_{ij} is the cost between task *j* and agent *i*. Also τ_{ij}^l is the pheromone trails for arc (i,j) for the objective, η_{ij}^l is the corresponding heuristic value, w_l is a weight rule thus takes the form:

$$\tau_{ij}^k(t+1) \leftarrow (1-\rho) w_k \tau_{ij}^k(t) + \sum_{a=1}^{r} \Delta\tau_{ij}^a,$$

where ρ is the evaporation rate of pheromone, $\rho \in [0, 1]$, r is the number of paths of ants, $\tau_{ij}(t+1)$ is the total pheromone deposit by ant on path (i, j) and $\Delta\tau_{ij}^{a}$ is the quantity of pheromone laid on the edge (i, j) by ant a. In ant colonies, pheromone intensity decreases over time because of evaporation. In MOACOA, evaporation is simulated by applying an appropriately defined pheromone evaporation rule:

$$\Delta\tau_{ij}^{a} = \begin{cases} \dfrac{1}{c_a}, & a^{th}\text{ant's assignment cost on the edge } (i, j), \\ 0, & \text{otherwise.} \end{cases}$$

This proposes the following process, depicted in the step-wise form, to obtain optimal assignment for an MOAP:

Step 1: Formulate the Assignment Cost Matrix (ACM) for each objective.

Step 2: Define the values of α, β, ρ, w_l and initial pheromone level (τ_{ij}^{0}).

Step 3: Determine the transition probability values (p_{ij}^{q}) for the first row of the linear aggregation ACM.

Step 4: Compute the CP and generate the RNs in the corresponding row.

Step 5: Find the shortest path for the first row of the linear aggregation ACM comparing the CP and RNs.

Step 6: Exclude the rows and columns of ACMs corresponding to the selected shortest path.

Step 7: If the shortest path cannot be found, update the pheromones and go to Step 3.

Step 8: If the shortest path is found, repeat the process for the remaining rows of ACMs.

A flowchart of the proposed algorithm is given in the Figure 1 below:

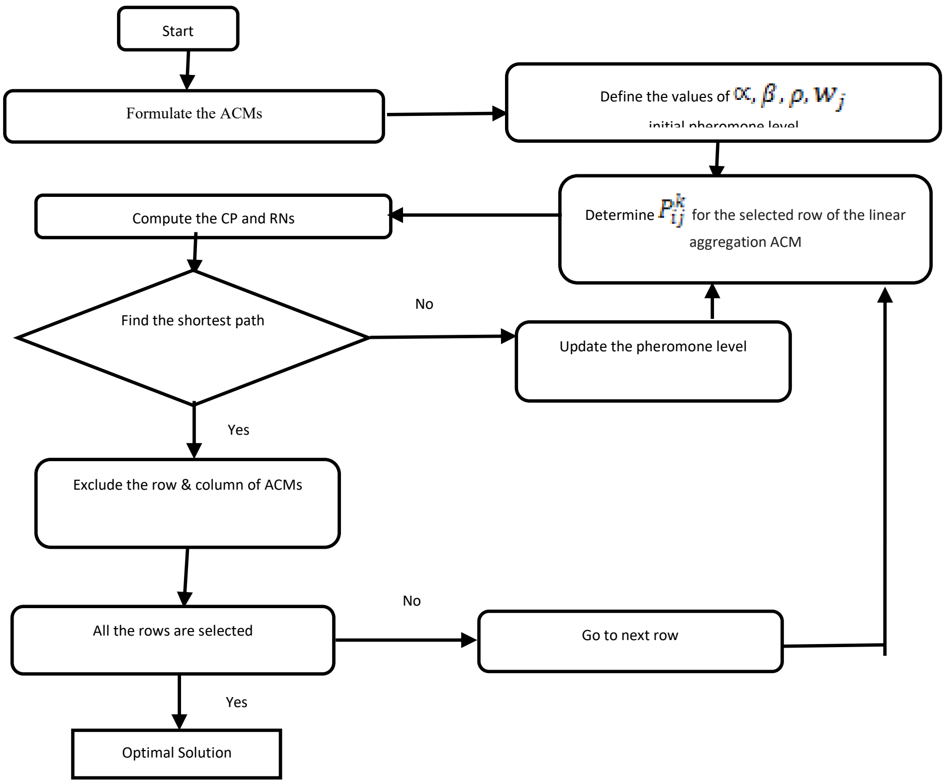

Figure 1. Flowchart of the proposed algorithm

The optimal solution obtained for the MOAP is evaluated using the TOPSIS method, which consists of the following steps:

Step 1: Formulate the Assignment Cost Matrix (ACM) for each objective.

Step 2: Define the values of w_j.

Step 3: Normalize the decision matrix for each objective.

Step 4: Compute the weighted normalized matrix.

Step 5: Determine the PIS and NIS.

Step 6: Calculate the Separation from the PIS and NIS for each alternative path.

Step 7: Compute the closeness coefficient for each alternative path.

Step 8: Rank the alternatives according to the closeness coefficient.

Step 9: Select the alternative with the highest rank as the best solution.

A flowchart of the TOPSIS method is given in the Figure 2 below:

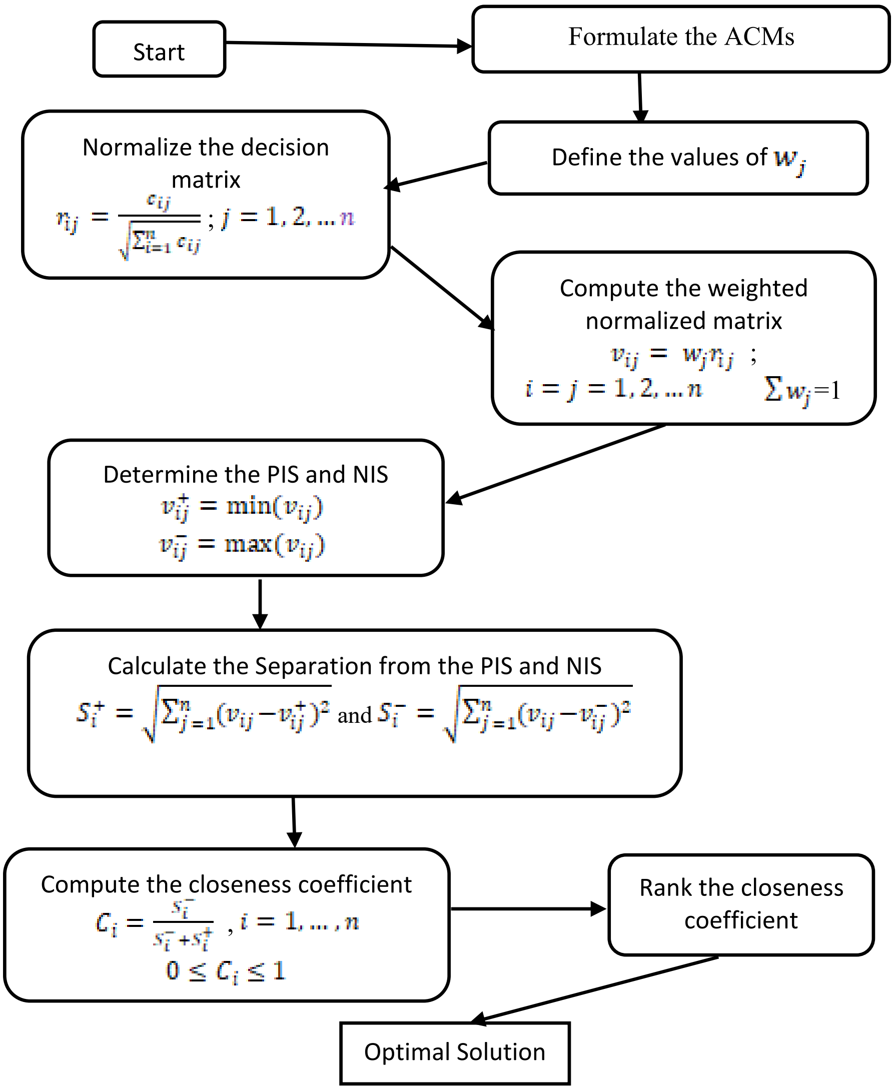

Figure 2. Flowchart of the TOPSIS method

RESULTS AND DISCUSSION

Illustration 1 with two objectives

This illustration, which consists of two objectives, considers four agents to be assigned for four tasks in the optimal manner, where assignment costs c_{ij} are randomly generated for the illustrative purpose, are given below in the matrix form, where c^1, c^2 are ACMs for the two objectives respectively:

$$c^1 = \begin{pmatrix} 77 & 6 & 62 & 7 \\ 39 & 72 & 95 & 59 \\ 34 & 82 & 27 & 6 \\ 75 & 42 & 27 & 77 \end{pmatrix} \quad \text{and } c^2 = \begin{pmatrix} 36 & 55 & 1 & 95 \\ 8 & 23 & 78 & 20 \\ 42 & 3 & 34 & 20 \\ 14 & 55 & 78 & 68 \end{pmatrix}$$

The MOAP can be formulated as below according to the notations defined earlier:

$$Min\, Z^k(x) = \sum_{i=1}^{4} \sum_{j=1}^{4} c_{ij}^k x_{ij}, \quad k = 1, 2.$$

subject to the constraints:

$$\sum_{j=1}^{4} x_{ij} = 1, \qquad i = 1, 2, 3, 4$$

$$\sum_{i=1}^{4} x_{ij} = 1, \qquad j = 1, 2, 3, 4$$

$$x_{ij} = \begin{cases} 1, & \text{if } i^{th} \text{resource assign to } j^{th} \text{task} \\ 0, & \text{if } i^{th} \text{ resource not assign to } j^{th} \text{ task.} \end{cases}$$

Since two objectives are considered, the transition probability can be rewritten as follows (Let $\alpha, \beta = 1$):

$$p_{ij}^k = \frac{(w_1 \tau_{ij}^1 + w_2 \tau_{ij}^2)(w_1 \eta_{ij}^1 + w_2 \eta_{ij}^2)}{\sum (w_1 \tau_{ij}^1 + w_2 \tau_{ij}^2)(w_1 \eta_{ij}^1 + w_2 \eta_{ij}^2)}$$

Without loss of generality we take $w_1 = 0.5$ and $w_2 = 0.5$ ($\sum_{i=1}^{2} w_i = 1$).

According to the proposed method given in the step-wise form, initially the first row of each of the ACMs is considered. Subsequently, the η_{ij}^1, η_{ij}^2 and transition probabilities for the paths are calculated in the first row of each ACM as shown in Table 1 below. The model is solved using ACOA coded in Python program and without loss of generality, let the initial pheromone value to be 1:

Table 1: Transition probability on the first rows of the ACMs

Path	1st row (c^1)	1st row (c^2)	τ_{ij}^1	τ_{ij}^2	η_{ij}^1	η_{ij}^2	$P_{i,j}^1$
$1 \to 1$	77	36	1	1	0.0130	0.0278	0.0292

$1 \to 2$	6	55	1	1	0.1667	0.0182	0.1325
$1 \to 3$	62	1	1	1	0.0161	1.0000	0.7283
$1 \to 4$	7	95	1	1	0.1428	0.0105	0.1099

Initially, the cumulative probabilities are computed, and the corresponding RNs are generated for the first row of the matrix obtained by the linear aggregation of the ACMs. Comparing the CP and the generated RNs, for example, if the random number 0.0619 is generated, the new path from $1 \to 2$ is selected by the ant, because the corresponding transition probability falls in the interval (0.0292, 0.1617), as shown in the column 4 of Table 2. Similarly, new paths are selected by comparing the random numbers and CP shown in the remaining columns in Table 2 below:

Table 2: Trasition probabilities and new paths of first rows of the respective ACM

Path	$P_{i,j}^1$	**Cumalative Probability**	**Path $1 \to 1$**	**Path $1 \to 2$**	**Path $1 \to 3$**	**Path $1 \to 4$**
$1 \to 1$	0.0292	0.0292	RN: 0.0619 and new path $1 \to 2$	RN: 0.1889 and new path $1 \to 3$	RN: 0.7255 and new path $1 \to 3$	RN: 0.3889 and new path $1 \to 3$
$1 \to 2$	0.1325	0.1617				
$1 \to 3$	0.7283	0.8900				
$1 \to 4$	0.1099	1.0000				

As shown in Table 2, the paths $1 \to 2$, $1 \to 3$, and $1 \to 4$ converge to the same path, that is $1 \to 3$, while the remaining path follows the path $1 \to 2$. In the subsequent step, the pheromone values (total pheromene) are updated for the newly selected paths, as presented in Table 3. During the second phase, the pheromone evaporation rate (ρ) is set to 0.5.

Table 3: τ_{ij}^1, τ_{ij}^2, η_{ij}^1 and η_{ij}^2 values for the first row in the second phase

Path	τ_{ij}^1	τ_{ij}^2	c_{ij}^1	η_{ij}^1	c_{ij}^2	η_{ij}^2
$1 \to 2$	0.2630	0.2778	6	0.1667	55	0.0182
$1 \to 3$	0.5756	1.2787	62	0.0162	1	1

The new transition probabilities for paths in the first row of each ACM in the second phase are calculated, and the results obtained are shown in Table 4 below:

Table 4: Paths for the first row in the second phase

Path	$P_{i,j}^2$	Cumulative Probability	Path $1 \to 1$	Path $1 \to 2$
$1 \to 2$	0.0504	0.0504	RN: 0.7630 and new path $1 \to 3$	RN: 0.7839 and new path $1 \to 3$
$1 \to 3$	0.9496	1.0000		

Subsequently, comparing the CP and the generated RNs as before, the path for the ants is selected. That is, the same path from $1 \to 3$ is taken for both paths $1 \to 2$ and $1 \to 3$. Therefore, the optimal assignment for the first row of the corresponding ACMs is determined as $1 \to 3$. The optimal solution for the first row of each ACMs is recorded. Subsequently, the row and column of each ACMs corresponding to the selected path are excluded. This procedure is then repeated for the remaining rows, and the optimal solution corresponding to each row is recorded. Finally, the proposed iterative technique converges to the optimal assignment for the MOAP.
The optimal assignment is {(1, 3), (2, 1), (3,4), (4, 2)} and the total assignment cost is calculated as:

$$\sum_{i=1}^{4}\sum_{j=1}^{4} c_{ij}^k x_{ij} = (62+1)+(39+8)+(6+20)+(42+55) = 63+47+26+97 = 233.$$

The TOPSIS method is an important multi-criteria decision-making (MCDM) approach for solving MOAP. It is one of the most widely used and conceptually simple method. The solution obtained using the TOPSIS method is

{{0, 0, 1, 0}, {1, 0, 0, 0}, {0, 0, 0, 1}, {0, 1, 0, 0}}.

From this result, the optimal assignment is {(1,3),(2,1),(3,4),(4,2)}, and the total assignment cost is 149 + 84=233. Hence, the result obtained by the proposed algorithm for the two objectives is verified using the TOPSIS method.

Illustration 2 with three objectives

This illustration, which consists of three objectives, considers four workers to be assigned for four jobs in the optimal manner, where assignment costs c_{ij} are randomly generated for the illustrative purpose, and are given below in the matrix form, where c^1, c^2, c^3 are ACMs for the three objectives respectively:

$$c^1 = \begin{pmatrix} 2 & 5 & 4 & 7 \\ 3 & 3 & 5 & 7 \\ 3 & 8 & 4 & 2 \\ 6 & 5 & 2 & 5 \end{pmatrix}, c^2 = \begin{pmatrix} 3 & 3 & 6 & 2 \\ 5 & 3 & 7 & 2 \\ 5 & 2 & 7 & 4 \\ 4 & 6 & 3 & 5 \end{pmatrix} \text{ and } c^3 = \begin{pmatrix} 4 & 2 & 5 & 3 \\ 5 & 3 & 4 & 3 \\ 4 & 3 & 5 & 2 \\ 6 & 4 & 7 & 3 \end{pmatrix}$$

Assignment model with three objectives

$$Z^k(x) = \sum_{i=1}^{4}\sum_{j=1}^{4} c_{ij}^k x_{ij}, \quad k = 1,2,3$$

subject to the constraints

$$\sum_{j=1}^{4} x_{ij} = 1, \qquad i = 1,2,3,4$$

$$\sum_{i=1}^{4} x_{ij} = 1, \qquad j = 1,2,3,4$$

$$x_{ij} = \begin{cases} 1, & \text{if } i^{th} \text{resource is assigned to } j^{th} \text{task} \\ 0, & \text{if } i^{th} \text{ resource is not assigned to } j^{th} \text{ task.} \end{cases}$$

Without loss of generality we take $w_1 = 0.4$, $w_2 = 0.3$ and $w_3 = 0.3$ ($\sum_{i=1}^{3} w_i = 1$). Here, using the MOACOA coded in Python programming language to solve the illustrative example with three objectives, the proposed iterative technique successfully converges to the optimal assignment of the MOAP. The optimal assignment is
{(1, 1), (2, 2), (3, 4), (4, 3)} and the total assignment cost is calculated as,

$$\sum_{i=1}^{4}\sum_{j=1}^{4} c_{ij}^{k} x_{ij} = (2 + 3 + 4) + (3 + 3 + 3) +(2 + 4 + 2) + (2 + 3 + 7) = 38.$$

As before, the optimal assignment obtained through the steps of the TOPSIS method is
{{1, 0, 0, 0}, {0, 1, 0, 0}, {0, 0, 0, 1}, {0, 0, 1, 0}}.
Based on this result, the corresponding optimal assignment is {(1, 1), (2, 2), (3, 4), (4, 3)}, yielding a total assignment cost of 9+ 9 + 8 + 12 = 38. Hence, the results obtained by the proposed algorithm for the illustration with three objectives is verified by the TOPSIS method.

Comparision of computational efficency between MOACOA and TOPSIS method in solving the MOAP

The proposed algorithm is coded in Python programming language and is verified using the TOPSIS method. The TOPSIS method is a well known traditional algorithm to solve MOAPs. This method attempts to reach the optimal solution in contrary to the MOACOA. In this study, the performances of the TOPSIS method and the MOACOA are evaluated in terms of computational time required to reach an optimal solution for the MOAP, by varying the matrix size from 2 to 10 for two and three objective functions. Table 5, which is given below, exhibits the results of the analysis. The last row of the table shows that the TOPSIS method fails to reach the optimal solution in both cases where the matrix size exceeds 11.

Table 5: A comparison of computational time between the MOACOA and TOPSIS method to solve MOAP

	Elapsed time (Seconds)			
Size of ACM	**Two objectives**		**Three objectives**	
	MOACOA	**TOPSIS Method**	**MOACOA**	**TOPSIS Method**
2	0.0339	1.2744	0.0479	1.3439

3	0.0663	1.2958	0.0635	2.0112
4	0.1371	1.4598	0.1442	2.2113
5	0.1930	1.4631	0.1995	3.3480
6	0.2400	2.4995	0.3305	4.4108
7	0.4499	2.8681	0.4086	4.4949
8	0.5079	4.3824	0.5861	6.2688
9	0.5123	5.3954	0.6224	8.9179
10	0.7101	34.9261	0.7682	47.0873
11	0.7346	-	0.7698	-

According to the Table 5 given above, the TOPSIS method requires significantly more computational time to solve the problem as the size of the problem increases. For example, when the order of the ACM is 10, the TOPSIS method takes as long as 34.9261 and 47.0873 seconds respectively to obtain the optimal solution for the two cases, whereas MOACOA produces the near optimal solution in only 0.7101 and 0.7682 seconds respectively. The Figure 3 below clearly illustrates the computational time required by each method in both cases:

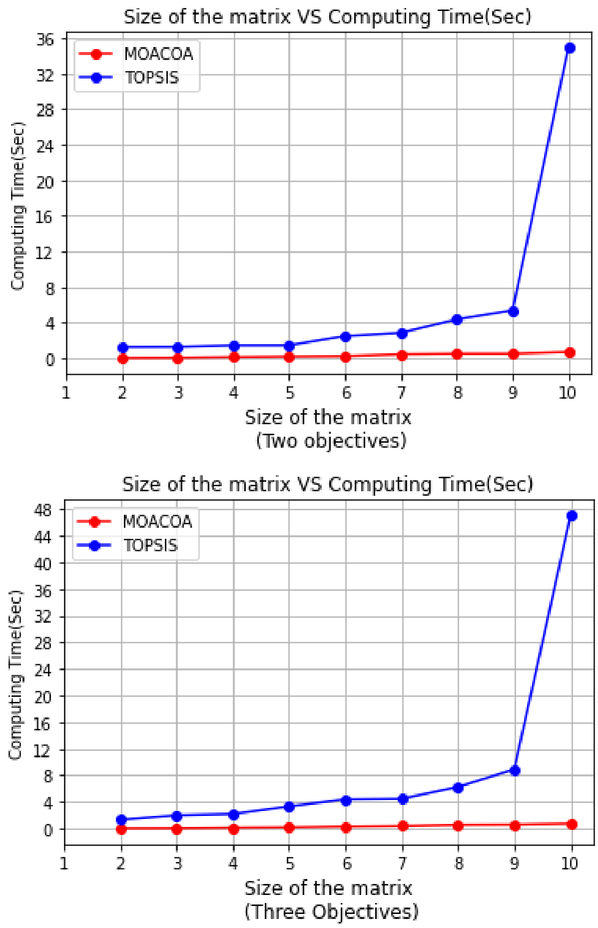

Figure 3. Size of the ACM vs Computational time (seconds) for two and three objectives

CONCLUSION

This study proposes a Multi-Objective Ant Colony Optimization Algorithm (MOACOA) for solving deterministic Multi-Objective Assignment Problems (MOAPs). The proposed algorithm, MOACOA, is coded in Python programming language and is verified its performances using the TOPSIS method. This proposed metaheuristic algorithm is capable of solving large scale MOAPs in less computational time compared to time taken by the TOPSIS method for the same. Table 5 shows that both algorithms provide identical assignments for small scale problems and MOACOA produced assignment solutions identical to those obtained by the TOPSIS method, confirming the accuracy and reliability of the proposed approach. The study shows the efficiency and robustness of MOACOA for solving real world large scale MOAPs. Hence, in this study it shows that for the constrained MOAPs, MOACOA stands out as a viable and smart solution that combines the maximum output and feasibility, which is optimal in circumstances where the TOPSIS method fails to be useful. Hence, TOPSIS becomes computationally less efficient or less practical for large-scale problems. This study recommends that the proposed method can be used more efficiently and effectively in solving large scale MOAPs.

The primary significance of this study is in the creation of the biologically-inspired heuristic framework that utilizes the combination of effective construction of the solutions and learning processes based on the pheromones for solving constrained MOAPs. This algorithm represents a valuable alternative to classical multi-criteria decision-making approaches in situations where the problem becomes computationally demanding.

Even though the current research focuses on deterministic scenarios only, the developed approach paves way for future studies concerning multi-objective assignment problems that involve uncertainties. Future studies may extend the proposed MOACOA to fuzzy, stochastic, and other uncertain multi-objective assignment models and investigate hybridization with other metaheuristic techniques to further improve solution quality and computational performance.

REFERENCE

[1] Alaya. I., Solnon. C., Gh´edira. K. (2007), Ant colony optimization for multi-objective optimization problems. In: 19th IEEE International Conference on Tools with Artificial Intelligence (ICTAI 2007), Los Alamitos, CA, vol. 1, pp. 450–457. IEEE, Computer Society Press, Los Alamitos.

[2] Alizadeh, B., Asghar Gholamian. S.A., (2014), Application of Ant Colony Optimization Algorithm for Optimal Design of Squirrel Cage Induction Moto, Journal of Mechatronics, Electrical and Computer Technology, Vol. 4(13), pp. 1674-1690.

[3] Behzadian, M., Otaghsara, S. K., Yazdani, M., & Ignatius, J. (2012). A state-of-the-art survey of TOPSIS applications. Expert Systems with Applications, 39(17), 13051–13069.

[4] Blum, C. (2005). Ant colony optimization: Introduction and recent trends. Physics of Life Reviews, 2(4), 353–373.

[5] Doerner. K., Gutjahr. W. J., Hartl, R. F., Strauss. C., Stummer. C. (2004). Pareto ant colony optimization: A metaheuristic approach to multi-objective portfolio selection. Annals of Operations Research 131, 79–99.

[6] Dorigo. M., Maniezzo,V., and Colorni, A. (1991).“Positive Feedback as a Search Strategy”, Technical Report 91-016, Dipartimento di Elettronica, Politecnico di Milano, Milan, Italy.

[7] Dorigo. M., (1992). Optimization, learning and natural algorithms. PhD thesis, Dipartimento di Elettronica, Politecnico di Milano.

[8] Dorigo. M, Di Caro. G, and Gambardella. L. M. (1999). Ant algorithm for discrete optimization, Artificial Life, MIT Press, 5137-72.

[9] Gulben. C, Orhan.Y,(2015), “An improved ant colony optimization algorithm for construction site layout problems”, Building construction and planning research, 3, 221-232.

[10] Hwang, Ching-lai and Yoon. (1981), Multiple Attribute Decision Making: Methods and Applications, Springer-Verlag, New York.

[11] Iredi. S., Merkle. D., Middendorf. M. (2001). Bi-criterion optimization with multi colony ant algorithms. In: Zitzler, E., Deb, K., Thiele, L., Coello, C.A., Corne, D.W. (eds.) EMO LNCS, vol. 1993, pp. 359–372. Springer, Heidelberg.

[12] Kantorovich. L., V. Etal. (1965), The best use of economic resources. The best use of economic resources.

[13] Manuel L, Thomas S. (2010), “An Analysis of Algorithmic Components for Multi-objective Ant Colony Optimization: A Case Study on the Bio-objective TSP”, Springer- Verlag Berlin Heidelberg, P. Collet et al. (Eds.): EA 2009, LNCS 5975, pp. 134–145.

[14] Monteriro. S. R., Dalila B. M. M. F., Fernando A. C. C. (2012). "Ant colony optimization: a literature survey", Economics and management, 474.

[15] Pathirana. C.P.S., Daundasekera. W.B, (2024), Applying Ant Colony Optimization Algorithm to Solve the Deterministic Single Objective Assignment Problem, Postgraduate Institute of Science (PGIS) Research Congress 2024, Volume 11, p58, 01st and 2nd November 2024.

[16] Rekaya. R., Robbins. K., Spangler. M., Smith. S., Hay. E. H., and Bertrand K. (2013). "Ant colony algorithm with applications in the field of genomics", Intech.

[17] Starkweather. T., McDaniel. S., Mathias. K, Whitley. D. (1991), A comparison of genetic sequencing operators, 4th International Conference on Genetic Algorithms (ICGA '91), University of California at San Diego, San Diego, pp 69-76.

[18] Syariza. S. F., Rahman. A and Rahman. R. A. (2018). "An Assignment Problem and Its Application In Education Domain: A Review and Potential Path", Hindawi, Advances in Operations Research, Volume, Article ID 8958393.

[19] White. D. J. A. (1984), special multi-objective assignment problem. Journal of the Operational research Society, 759–767.

Characterization of Domestic Auto Diesel Adulteration with Kerosine up to 20%

J. A. C. P.Jayasinghe*, R. C. L. De Silva, D. A. D.I. Sewwandi, M. I. Mallikaratchy

Petroleum and Lubricant Testing Laboratory, Industrial Technology Institute, Colombo 07.

ABSTRACT

As the fuel prices escalates fuel adulteration incidences are reported in domestically and diesel adulteration is most prominently reported specially in private transportation sector. This research was carried out to characterize and estimate the diesel adulteration with kerosine at a maximum range up to 20%. Domestic Diesel and kerosine samples obtained from a fuel station. Parameters: distillation, flash point viscosity were analyzed using ASTM methods. Further more blended samples were analyzed using FTIR to find out their chemical structures. Samples were blended in volume-to-volume ratios. Control samples were taken as original diesel sample and original kerosine sample that taken from fuel station. Samples were prepared as 5K (5% Kerosine + 95% Diesel), 10K (10% Kerosine + 90% Diesel), 15K (15% Kerosine + 85% Diesel), 20K (20% Kerosine + 80% Diesel). According to results, increasing the concentration of kerosene in the blends decreases the kinematic viscosity and IBP in distillation and flash point values of the blended fuel compared with authentic diesel, but increases these values compared with authentic kerosene. Authentic diesel flashed at 86°C, while kerosene flashes at 47.5°C. just adulterating even 5% kerosene causes a colossal 10.5°C drop (down to 75.5°C). By the time adulteration reaches 20%, the flash point plummets to 68.5°C. A lower flash point increases the risk of premature ignition and adversely effects the engine performance. Impact of adulteration observed every 5% increment of kerosene methodically reduces the viscosity (from 3.794 → 3.522 → 3.346 → 3.093 → 3.000 cSt). Fuel pumps and injectors rely on the viscosity of diesel for lubrication. Thinner, low-viscosity fuel resulting from kerosene adulteration could result with increase in friction, fuel pump wear, and injector leakage could be possible. Distillation Profile (IBP and 50% Recovery) Initial Boiling Point (IBP): Authentic diesel boiled at 186.6°C, while kerosene at 161.2°C. When kerosene is added to diesel, the IBP experiences an immediate drop to 185.2°C at a 5% blend, and steadily declines to 175.0°C at a 20% blend. 50% Recovery Temperature (T_{50}): This parameter shows a highly predictable, linear decline. Pure diesel's mid-boiling point is 292.6°C. As kerosene is blended in at 5%, 10%, 15%, and 20%, the T_{50} temperature drops systematically to 289.0°C, 286.8°C, 281.9°C, and 277.7°C correspondingly. There is not very much significance difference between blended samples and control samples. Since the differences between pure diesel and pure kerosene are structural (chain lengths and branching) rather than functional (they contain the same elements), *new* peaks appearing or disappearing was not observed. Overall results shows that diesel adulteration adversely affects on engine performance.

Keywords: Adulteration, Diesel, Kerosine, Distillation, Flashpoint

----

*chathu1995jaya@gmail.com

INTRODUCTION

Diesel adulteration is a thriving business throughout the globe specially in the Asian region with the existence of significant price differences seen with fuel compared to the adulterants. Establishment of a routine analysis methodology with minimum sample handling steps and absence of cumbersome sample preparation, and separation processes seems to be the most viable solution in monitoring and quantifying the fuel adulterants (Kulathunga & Mahanama, 2013).

Sri Lanka as an Asian country was also affected with escalating price hikes at close frequencies.

These days oil prices are changing mainly due to several factors, including international war, policies of oil-exporting countries, security, the world political situation, and many other natural factors such as depletion of petroleum reserves.

In this light consuming fuel at routine has become costly with an economic burden. Recently several cases were reported specially some private buses were caught on diesel adulteration with adulterant-kerosine.

The literature related to the effect of kerosene on diesel fuel properties shows that kerosene improves the cold flow characteristics of diesel fuel by simply diluting the problematic paraffin waxes present in the diesel fuel distillation curve. Baral & Robert (2009), have reported that the density of the kerosene-diesel blend remains within the prescribed limit even in higher blends and also kinematic viscosity of the blends were decreased with an increase in blend ratio. Bergstrand (2004), has reported that kerosene has a lower cetane number than diesel and giving a longer ignition delay. In Sri Lanka, it is very common that blending small amount of kerosine with diesel to the engine.

Having similar chemical properties, the fuel and the adulterant cannot be distinguished easily leading to complications in identification and quantification of the adulterants. A number of analytical techniques are available ranging from simple density measurements to modern techniques such as gas chromatography/mass spectroscopy for identification of adulterants. The common testing methods for the fuels are density measurements, rate of evaporation, ash content determinations and viscosity measurements (Kalligeros et al., 2003), optical sensors, spectroscopic methods (Canizares & de Castro, 1996; Patra & Mishra, 2001).

The main objective of this study is to characterize the domestically available main auto diesel adulteration with domestically available kerosine using basic parameters: flash point, Kinematic viscosity, Distillation- Initial boiling point (IBP). Further Fourier Transform Infrared Spectroscopy (FTIR) characterization was also used in characterization.

METHODOLOGY

Commercial auto diesel fuel and the kerosene were purchased from local commercial fuel station. The conventional diesel fuel was blended with kerosene in different proportions by manual mixing at room temperature. In this study, 5%, 10%, 15% and 20% kerosene (by volume) were adulterated on auto diesel and denoted hereafter as 5K, 10K, 15K and 20K respectively.

The authentic diesel and authentic kerosene were denoted as D100 and K100, respectively. Properties namely kinematic viscosity, flash point and distillation profile were measured in the laboratory according to the ASTM test methods. Structural changes were investigated by FTIR method. These physiochemical properties are shown in Table 1.

Meterial's flash point is regarded as the lowest temperature at which a liquid produces sufficient vapor to ignite when exposed to a source of ignition. It is regarded as a critical safety characteristic that supports classify flammable liquids, with fuels having a flash point less than 37.8 °C (100.0 °F) considered flammable, while those above this temperature are classified as combustible. Flash point is important for the safe handling and storage of flammable substances, as it designates the potential fire hazards associated with a fuel as well as the degree of combustion in the engine which are potential consequences of using diesel fuel with a low flash point. While engine performance may be affected, the primary concern lies in the safety hazards of handling and transporting the out-of-spec fuel. Lower flash points increase the risk of explosions, making it crucial to address the issue promptly and appropriately. The lower the flash point, the more the risk is increased.

Finding a solution to a low flash point is challenging. While some may consider adding substances to raise the flash point, this approach often adversely affects other fuel properties. Dilution with additional diesel fuel is also impractical, as large volumes would be required to rectify the flash point issue (Bell performance, 2026).

ASTM D 3828-169(2021) method was used for flashpoint testing and SETA:U82000-2U Automatic high temperature closed cup flashpoint tester was used to test the samples.

Viscosity is the resistance to shear or flow in a fluid - and a measure of the adhesive/cohesive or frictional property. Viscosity arising due to internal molecular friction produces the frictional drag effect (Engineering ToolBox, 2001). Kinematic viscosity (ν) is defined as the ratio of dynamic viscosity (η) to the density (ρ) of the fluid. It is typically measured in centistokes (cSt) or square millimeters per second (mm^2/s). The kinematic viscosity of oil is crucial for understanding how it will perform in various applications, particularly in engines and machinery.

Kinematic viscosity was measured using SETA KV-6 viscometer bath and adopting ASTM D 445-24. The Initial Boiling Point (IBP) in distillation is the temperature at which the first drop of vaporized liquid is collected from a mixture as it is heated. Unlike pure substances, which have a single boiling point, complex mixtures such as crude oil or petroleum products boil over a range of temperatures. The IBP marks the start of this boiling range and is critical for understanding the volatility and composition of the mixture.

ASTM D 86-239 method was adopted to measure the samples using Thanaka ad-7 automated atmospheric distillation tester

RESULTS AND DISCUSSION

According to Table 1, increasing the concentration of adulterant- kerosene in the blends decreases the kinematic viscosity and IBP in distillation and flash point values of the blended fuel compared with authentic diesel, but increases these values compared with authentic kerosene.

Table 1: Flash point (^{0}C)/ kinematic viscosity/ Distillation-IBP/ Distillation- Rec. 50%

Fuel blend	Flash point (^{0}C)	kinematic viscosity (cSt)	Distillation-IBP (Initial boiling point) ^{0}C	Distillation-Recovery percentage. 50% (^{0}C)
(Unadulterated Diesel) D100	86	3.794	186.6	292.6
K100 (Unadulterated Kerosine)	47.5	1.260	161.2	194.8
5% kerosene on Diesel	75.5	3.522	185.2	289.0
10% kerosene on Diesel	74	3.346	178.3	286.8
15% kerosene on Diesel	70.5	3.093	178.1	281.9
20% kerosene on Diesel	68.5	3.000	175.0	277.7

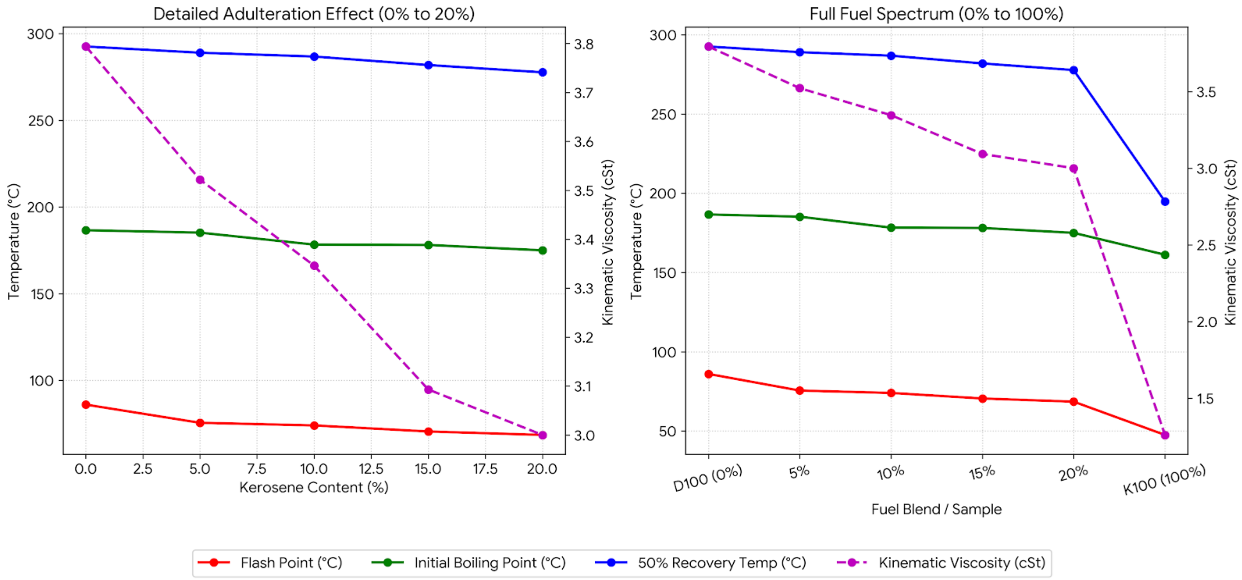

Figure 1: Multi-Curve Analysis of Diesel Fuel Properties under Progressive Kerosene Adulteration

According to the Table 1, and Figure 1the flash point drops suddenly with the introduction of even small amounts of kerosene. Unadulterated diesel observed flashing at 86°C, while unadulterated kerosene flashes at 47.5°C. just adulterating even 5% kerosene causes a colossal 10.5°C drop (down to 75.5°C). By the time adulteration reaches 20%, the flash point plummets to 68.5°C.
Flash point is a critical safety metric for fuel handling and storage. A lower flash point increases the risk of premature ignition and adversely effects the engine performance.

Kinematic Viscosity decreases linearly when kerosene percentage increases. Diesel stands at a higher viscosity, whereas kerosene is much thinner in viscosity comparatively. Impact of adulteration observed every 5% increment of kerosene methodically reduces the viscosity (from 3.794 → 3.522 → 3.346 → 3.093 → 3.000 cSt).
Fuel pumps and injectors rely on the viscosity of diesel for lubrication. Thinner, low-viscosity fuel resulting from kerosene adulteration could result with increase in friction, fuel pump wear, and injector leakage could be possible.

Distillation Profile (IBP and 50% Recovery) Initial Boiling Point (IBP): Pure diesel commences boiling at 186.6°C, while pure kerosene commences at 161.2°C. When kerosene is added to diesel, the IBP experiences an immediate drop to 185.2°C at a 5% blend, and steadily declines to 175.0°C at a 20% blend. 50% Recovery Temperature (T_{50}): This parameter shows a highly predictable, linear decline. Pure diesel's mid-boiling point is 292.6°C. As kerosene is blended in at 5%, 10%, 15%, and 20%, the T_{50} temperature drops systematically to 289.0°C, 286.8°C, 281.9°C, and 277.7°C correspondingly.
Reduction in distillation temperatures demonstrates that the overall fuel mixture is becoming lighter and more volatile. This disrupts the engine’s designed combustion timing, reducing thermal efficiency and potentially increasing harmful emissions.

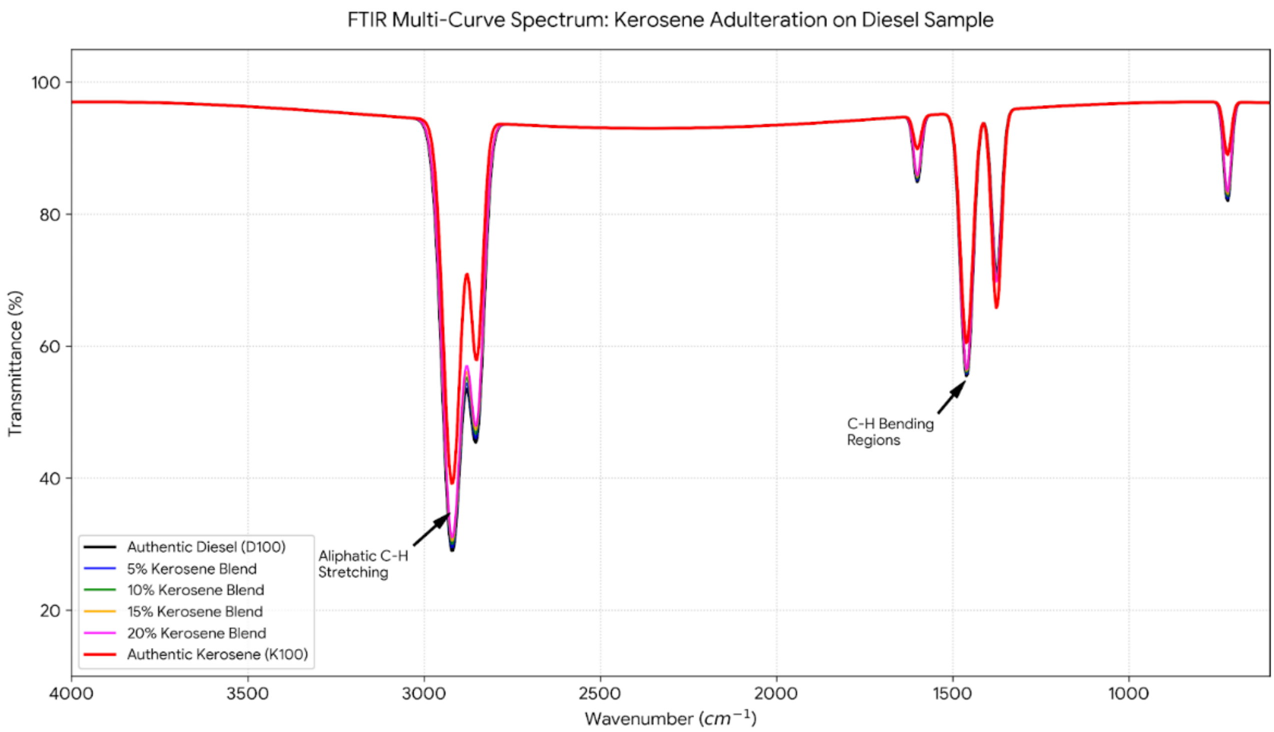

Figure 2: Multi-Curve FTIR Analysis of Diesel Kerosene Adulteration

According to FTIR analysis Significant peaks were observed between 2856 cm -1 and 2936 cm -1, corresponding to the C-H stretching vibrations of methylene (CH2) and methyl (CH3) groups, which are typical for alkanes. The wavelengths between 1451 -1460 cm^{-1} CH_2 bending, and at 1165 -1175 cm^{-1} C-O vibrations can be identified. There is not very much significance difference between blended samples and control samples. Since the differences between pure diesel and pure kerosene are structural (chain lengths and branching) rather than functional (they contain the same elements), *new* peaks appearing or disappearing was not observed.

Instead, the adulteration behaves as a systematic dilution framework. The Figure 2 tracks a mathematically consistent shift in peak heights and area ratios—most reliably at the1375 cm^{-1} methyl bend and the 720 cm^{-1} long-chain.

CONCLUSION

The experimental data clearly demonstrates that kerosene adulteration severely degrades the physical and chemical properties of diesel fuel. High Sensitivity of Flash Point: Flash point is the most immediate indicator of low-level contamination. A simple 5% addition of kerosene compromises fuel safety specifications significantly. Predictable Linear Degradation: Kinematic viscosity and the 50% Distillation Recovery temperature drop in direct, predictable proportion to the amount of kerosene added. This makes them highly reliable metrics for quantifying the exact percentage of adulteration in a suspect sample. Operational Risks: Ultimately, using diesel adulterated with kerosene (even as low as 5% to 20%) will lead to reduced engine lubrication, accelerated component wear, altered combustion cycles, and elevated safety risks due to heightened fuel volatility

A lower flash point may increase the risk of premature ignition and adversely effects the engine performance. Fuel pumps and injectors rely on the viscosity of diesel for lubrication. Thinner, low-viscosity fuel resulting from kerosene adulteration could result with increase in friction, fuel pump wear, and injector leakage could be possible. Reduction in distillation temperatures demonstrates that the overall fuel mixture is becoming lighter and more volatile. This disrupts the engine’s designed combustion timing, reducing thermal efficiency and potentially increasing harmful emissions. Further testing is proposed as future work to conclude the overall effects of diesel adulteration with kerosine.

REFERENCE

[1] Kulathunga, Rashmi & Mahanama, Ranjith. (2013). Fingerprinting diesel and petrol fuels for adulteration in Sri Lanka. Journal of the National Science Foundation of Sri Lanka. 41. 287. 10.4038/jnsfsr.v41i4.6247.

[2] Bivek, Baral & Raine, Robert. (2009). Performance and Emissions of a Spark Ignition Engine Running on Gasoline Adulterated with Kerosene. SAE Technical Papers, 10.4271/2009-28-0014. DOI:10.4271/2009-28-0014.

[3] Bergstrand (2004) The Effects of Orifice Shape on Diesel Combustion. Bergstrand - 2004 - The Effects of Orifice Shape On Diesel Combustion | PDF | Fuel Injection | Exhaust Gas

[4] Kalligeros, S., Zannikos, F., Stournas, S., Lois, E., Anastopoulos, G., Teas, C., & Sakellaropoulos, F. (2003). An investigation of using biodiesel/marine diesel blends on the performance of a stationary diesel engine. Biomass & Bioenergy, 24, 141-149.

[5] Canizares, P, & Luque de Castro, M D.(1996) Flow-through sensor based on derivative synchronous fluorescence spectrometry for the simultaneous determination of pyrene, benzo(e)pyrene and benzo(ghi)perylene in water. Germany.

[6] D. Patra and A. Mishra(2001)., "Excitation Emission Matrix Spectral Subtraction Fluorescence to Check Adulteration of Petrol by Kerosene," Appl. Spectrosc. 55, 338-342

[7] Bell performance (2026).[online] Understanding Flash Point: Ensuring Fuel Safety and Performance. https://www.bellperformance.com/bell-performs-blog/understanding-flash-point-ensuring-fuel-safety-and-performance

[8] Engineering ToolBox (2001) [online].Liquids - Kinematic Viscosities https://www.engineeringtoolbox.com/kinematic-viscosity-d_397.html

[9] Onojowho, E.E. and Sadjere, G.E., (2024). Investigation of Effects of Kerosene Variation on a Tertiary Blended Biodiesel Powered Internal Combustion Engine Performance and Emission. *Green Energy and Environmental Technology*.

[10] Jati, J.F. and Bhikuning, A., (2022), November. Fuel parameter analysis from kerosene blended with biodiesel and diesel fuel. In *IOP Conference Series: Earth and Environmental Science* (Vol. 1104, No. 1, p. 012036). IOP Publishing.

[11] Patil, K.R. and Thipse, S.S., (2016). The effect of injection timing on the performance and emission of direct injection CI engine running on diethyl ether-diesel blends. *International Journal of Automotive and Mechanical Engineering*, *13*(3), pp.3773-3787.

[12] Akash, B.A., (2015). Combustion and emission investigation of diesel fuel and kerosene blends. *Research Journal of Applied Sciences, Engineering and Technology*, *10*(6), pp.618-622.

[13] Dorris, E., (1988). Additives for middle distillate and kerosine fuels. *Distillate Fuel: Contamination, Storage, and Handling*, *1005*, p.105.

[14] Fenstermaker, R.W. and Riley, R.K., (1984). Additives for improving the low-temperature filterability of diesel fuel oils. *SAE transactions*, pp.914-921.

ISSN 1391-0256

Journal of the Sri Lanka Association for the Advancement of Science

Volume 8 Issue 1

9771391025002